

---

# TimelyFreeze: Adaptive Parameter Freezing Mechanism for Pipeline Parallelism

---

Seonghye Cho<sup>1</sup> Jaemin Han<sup>1</sup> Hyunjin Kim<sup>1</sup> Euisoo Jung<sup>1</sup> Jae-Gil Lee<sup>1</sup>

## Abstract

Pipeline parallelism enables training models that exceed single-device memory, but practical throughput remains limited by pipeline bubbles. Although parameter freezing can improve training throughput by adaptively skipping backward computation, existing methods often *over-freeze* parameters, resulting in unnecessary accuracy degradation. To address this issue, we propose **TimelyFreeze**, which models the pipeline schedule as a directed acyclic graph and solves a linear program to compute *optimal* freeze ratios that minimize batch execution time under accuracy constraints. Experiments show that TimelyFreeze achieves up to 40% training throughput improvement on LLaMA-8B with comparable accuracy. Overall, it enables faster large-scale model training without compromising convergence and generalizes across diverse pipeline-parallel settings.

## 1. Introduction

Driven by scaling laws (Kaplan et al., 2020), deep learning models and datasets have grown beyond the capacity of a single GPU, making distributed learning indispensable for large-scale training. Among parallelization strategies, including data parallelism (DP) (You et al., 2018; Sergeev & Del Balso, 2018), tensor parallelism (TP) (Shoeybi et al., 2019), and pipeline parallelism (PP) (Huang et al., 2019), *pipeline parallelism* has emerged as a crucial technique for scaling model training. Unlike DP, which replicates the model across devices, PP splits the model into sequential stages, enabling memory-efficient scaling. Compared to TP, PP incurs lower communication overhead and is better suited to environments with limited inter-node bandwidth.

However, PP suffers from *training inefficiency* due to the inherently sequential nature of forward and backward computations. Each partitioned model stage must wait for preceding stages to complete their computations, creating idle

periods of computational resources (e.g., GPUs), commonly known as *pipeline bubbles*. To mitigate this inefficiency, various scheduling algorithms, such as GPipe (Huang et al., 2019) or 1F1B (Fan et al., 2021; Narayanan et al., 2019) have been proposed to improve hardware utilization. Nevertheless, pipeline bubbles persist, often leading to lower training throughput than data parallelism.

To improve training throughput, *parameter freezing* (Chen et al., 2023; Brock et al., 2017) has emerged as an effective approach, particularly in parameter-efficient fine-tuning and federated learning. By adaptively skipping backward computations and gradient updates for a subset of parameters, it reduces computational cost and improves training throughput. Nonetheless, parameter freezing may degrade accuracy due to skipped gradient updates in exchange for higher throughput. Moreover, prior methods (Chen et al., 2023; Liu et al., 2021) do not account for pipeline-parallel training dynamics and thus tend to apply excessive freezing, which unnecessarily degrades the model accuracy. For example, the gray region labeled “Ineffective Freezing” in Figure 1(b) illustrates a case where GPU 1–3 freeze parameters during the backward pass even though subsequent execution cannot yet begin due to schedule dependencies. As a result, such excessive freezing under PP neither improves throughput nor preserves training stability. Therefore, achieving an optimal balance between accuracy and throughput while accounting for pipeline-parallel training dynamics is crucial.

In this paper, we propose **TimelyFreeze**, a pipeline-aware parameter freezing method that balances accuracy and throughput in pipeline-parallel training. As indicated by the “Calibrated Backward Pass” region in Figure 1(c), it controls freezing by considering idle time in later execution block, or even increases freezing in the computational bottlenecks to balance computation across GPUs. By explicitly modeling pipeline schedules as directed acyclic graphs and optimizing freeze ratios accordingly, TimelyFreeze preserves accuracy more effectively while achieving better throughput.

We validate our method on the LLaMA series (1B/8B/13B) across pipeline schedules. TimelyFreeze lies on or near the Pareto frontier along two key axes—accuracy and throughput—achieving up to 46% throughput improvement with comparable or higher accuracy than baselines. More-

<sup>1</sup>School of Computing, KAIST, Daejeon, South Korea. Correspondence to: Jae-Gil Lee <jaegil@kaist.ac.kr>.

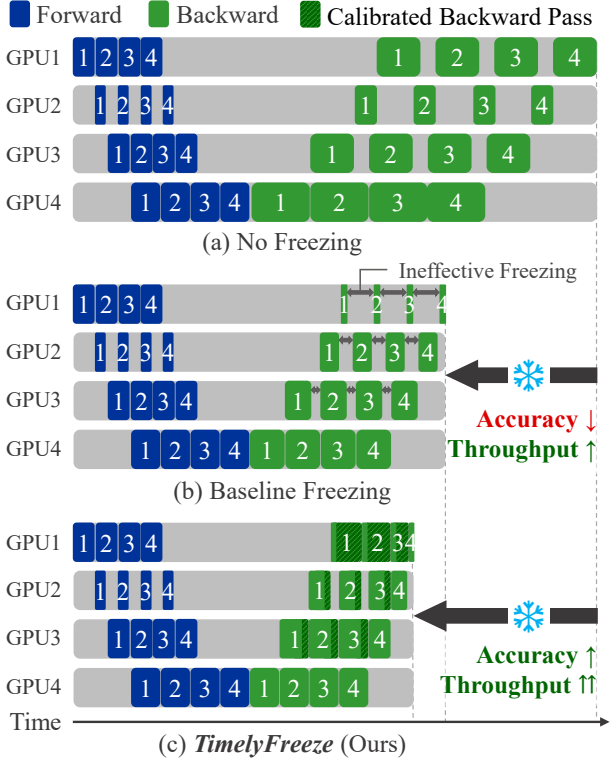


Figure 1. Effect of parameter freezing on pipeline parallelism. Each block denotes a microbatch execution in the forward (blue) or backward (green) pass. TimelyFreeze in (c) maintains the throughput gain of the baseline freezing method in (b) while preserving accuracy by effectively freezing according to the pipeline schedule.

over, TimelyFreeze generalizes to vision architectures (ViT-L/32 and ConvNeXtV2-L), reducing training time by up to 25% while keeping accuracy drops within 1.5 percentage points relative to the no-freezing baseline.

Collectively, these results demonstrate that TimelyFreeze robustly accelerates training across diverse pipeline-parallel settings, spanning different model architectures, scales, model partitioning heuristics, and hardware configurations. This work entails substantial, in-depth *system-oriented* research that directly impacts model training performance.

Our key contributions are summarized as follows:

- **Pipeline-aware freezing:** We reduce unnecessary freezing by leveraging runtime GPU idle time that arises from execution dependencies in pipeline schedules.
- **DAG-based formulation:** We represent pipeline schedules as directed acyclic graphs and derive expected freeze ratios by solving a linear program.
- **Time-to-accuracy analysis:** We provide a theoretical analysis of time-to-accuracy, characterizing the trade-off between throughput and convergence.

## 2. Preliminary and Related Work

### 2.1. Pipeline Parallelism

Pipeline parallelism partitions a model across multiple devices, enabling training of large-scale models that exceed the memory capacity of a single GPU. By splitting computation into sequential stages, it alleviates memory constraints and accelerates training, and various scheduling strategies have been proposed to maximize throughput.

**GPipe.** *GPipe* (Huang et al., 2019) divides a batch into smaller microbatches, enabling different pipeline stages to be executed concurrently across multiple GPUs. However, *GPipe* still suffers from notable underutilization due to pipeline bubbles and incurs an activation memory overhead that grows linearly with the number of microbatches.

**1F1B.** *1F1B* (1-Forward 1-Backward) (Narayanan et al., 2019; Fan et al., 2021) interleaves forward and backward computations. By performing a backward pass immediately after the forward pass, *1F1B* limits the accumulation of activations and reduces memory overhead. Nevertheless, *1F1B* schedule still suffers from low GPU utilization similarly to *GPipe*. Subsequently, to further improve utilization, *Interleaved 1F1B* (Narayanan et al., 2021) divides each stage into multiple micro-stages.

**Zero-Bubble.** Recent work such as *Zero-Bubble* (Qi et al., 2023; 2024) decomposes backward computations into finer-grained units to maximize GPU utilization, approaching near 100% utilization. However, this approach introduces additional communication and synchronization overhead, which can limit practical scalability, especially in heterogeneous or bandwidth-constrained environments.

### 2.2. Parameter Freezing

*Parameter freezing* is a training acceleration technique that selectively skips backward computations for a subset of model parameters to reduce training time. Prior work has focused on designing stability metrics to determine which parameters to freeze and when, aiming to minimize accuracy loss while maximizing computational efficiency.

**Monotonic Freezing from Front Layers.** Early approaches (Brock et al., 2017; Lee et al., 2019) rely on the empirical observation that *front layers tend to converge earlier than deeper layers*, and thus employ monotonic prefix freezing that freezes layers sequentially from the front to the back. Brock et al. (2017) progressively freeze shallow layers using predefined schedules, reducing computational cost in CNN models. Liu et al. (2021) and Wang et al. (2023) calculate layer-level stability metrics to determine the depth of the frozen prefix. Both methods also cache intermediate activations for the frozen layers, skipping not only backward passes but also redundant forward passes.

**Non-Monotonic Freezing.** More recent work (Li et al., 2024) questions the depth-ordered convergence assumption and proposes *non-monotonic* strategies. Li et al. (2024) observe that, due to residual connections, later layers may stabilize earlier than some intermediate layers. Chen et al. (2023) further increase granularity by performing parameter-wise freezing in federated learning, using gradient-based stability to reduce communication between clients and the central server. These methods relax the strict prefix constraint and thus offer greater flexibility.

However, prior freezing methods generally do *not* account for the characteristics of pipeline parallelism. As illustrated in Figure 1(b), when applied to pipeline-parallel settings, such pipeline-unaware designs can lead to unnecessary freezing that is misaligned with the pipeline execution timeline. PipeTransformer (He et al., 2021) partly addresses this issue by introducing dynamic load balancing. However, it permanently freezes parameters once selected, which introduces a non-negligible risk of accuracy degradation.

### 2.3. Baseline Freezing Methods

We select AutoFreeze (Liu et al., 2021) and APF (Chen et al., 2023) as our baselines, respectively representing the monotonic and non-monotonic freezing methods. Both methods are among the most widely cited in this area.

**AutoFreeze.** AutoFreeze estimates layer stability via the *gradient-norm change* for each layer and freezes layers in prefix order under the assumption that earlier layers converge faster. The gradient norm change for each layer at the  $K$ -th stability check is defined as

$$\text{Score}_{\text{Auto}, K} = \frac{\|\Delta_{K-1}\| - \|\Delta_K\|}{\|\Delta_{K-1}\|}, \quad (1)$$

where  $\Delta_K$  denotes the cumulative parameter update since the  $(K-1)$ -th check. A layer is frozen when (i) all preceding layers are already frozen and (ii) its gradient-norm change falls into the lower  $P_{\text{Auto}}$ -th percentile among all layers, controlled by a hyperparameter  $P_{\text{Auto}}$ .

**APF.** APF identifies parameters whose gradient updates oscillate without a clear trend as sufficiently stabilized and freezes them to reduce computation. To quantify such oscillatory behavior, APF computes the *effective perturbation score* for each parameter at the  $K$ -th stability check as

$$\text{Score}_{\text{APF}, K} = \frac{|E_K|}{E_K^{\text{abs}}}, \quad \begin{cases} E_K = \alpha E_{K-1} + (1 - \alpha) \Delta_K, \\ E_K^{\text{abs}} = \alpha E_{K-1}^{\text{abs}} + (1 - \alpha) |\Delta_K|. \end{cases} \quad (2)$$

Parameters whose score falls below the threshold  $T_{\text{APF}}$  are considered sufficiently stable and frozen.

## 3. Proposed Framework: TimelyFreeze

TimelyFreeze targets time efficiency and model performance preservation in practical pipeline parallel settings. To handle dynamic real world environment, we determine *freeze ratios*—how many parameters to freeze—in a fine-grained manner, per microbatch and per stage in the pipeline schedule. Through the overall training process, our method applies step-level parameter freezing through three phases: (1) *Warm-up and Monitoring* (Section 3.1), (2) *Freeze Ratio Formulation* (Section 3.2), and (3) *Freezing* (Section 3.3).

(1) During the monitoring phase, the system measures the GPU execution time for each forward and backward action, where each action corresponds to a unit of microbatch execution at a pipeline stage. (2) Based on these runtime measurements, TimelyFreeze constructs a graph representation of the pipeline schedule, which is then used to formulate a linear program that computes the expected freeze ratios  $r^*$ . (3) In the subsequent freezing phase, each backward action  $v_i$  starts freezing its corresponding parameters at  $r_i$ .

**Example.** As an illustrative example, the right gray box in Figure 2 shows a case where the batch time is reduced to about 70% of the original (left gray box), by freezing backward actions according to the expected freeze ratios computed in the previous phase (white box). In this example, each backward action has its own expected freeze ratio, with an average expected freeze ratio of 60%.

**Notation.** To be clear, let  $t$  denote the training step and  $\{T_w, T_m, T_f\}$  be the last step of the warm-up phase, the monitoring phase, and the progressive freezing phase, respectively. The notation is summarized in Appendix A.

### 3.1. Phase I: Warm-up and Monitoring

We employ an explicit *warm-up* phase at the beginning of training, as monitoring is only meaningful after CUDA kernel execution has stabilized. Accordingly, both monitoring and parameter freezing are disabled for the first  $T_w$  steps. We align  $T_w$  with the learning-rate warm-up steps, since the parameter updates during learning-rate ramp-up are highly unstable and even mild freezing can suppress critical early updates, destabilizing training. Freezing is therefore activated only after the learning-rate warm-up completes.

Once warm-up ends ( $t > T_w$ ), the system starts recording the execution time of every forward and backward action on each GPU in a two-part monitoring phase. During the first half, no parameters are frozen so that each action’s maximum backward duration can be measured (i.e., *upper-bound monitoring*). In the next half, all parameters are frozen to capture the minimum achievable latency (i.e., *lower-bound monitoring*). After samples for both bounds are collected (at step  $t = T_m$ ), the freeze ratios  $r$  are computed by solving the linear program described in Section 3.2.

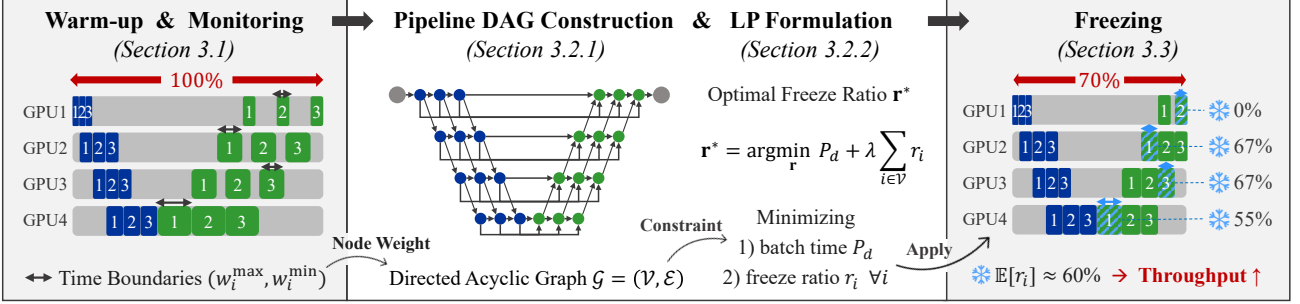


Figure 2. Method overview of TimelyFreeze. The system first monitors the upper and lower bounds of execution times and represents the pipeline schedule as a directed acyclic graph (DAG), where nodes and edges respectively denote action blocks and execution dependencies. Based on the DAG constraints, it solves a linear program to compute the expected freeze ratios  $r^*$ . Finally, it freezes each action block at its corresponding freeze ratio to improve training throughput while preserving accuracy.

### 3.2. Phase II: Freeze Ratio Formulation

At the end of the monitoring phase ( $t = T_m$ ), TimelyFreeze formulates a linear program (LP) based on the GPU execution time measurements of actions. The objective of this LP is to compute the *expected freeze ratio* for each action.

To ensure broad applicability across pipeline schedules and training settings, we represent the pipeline execution schedule of a batch as a directed acyclic graph (DAG), as described in Section 3.2.1. Building on this representation, we formulate a linear program that selects freeze ratios for actions to maximize training throughput while minimizing unnecessary parameter freezing, as detailed in Section 3.2.2.

#### 3.2.1. PIPELINE DAG CONSTRUCTION

**Pipeline DAG Nodes.** Let  $\mathcal{G} = (\mathcal{V}, \mathcal{E})$  be a directed acyclic graph (DAG) representing the pipeline schedule of a batch. The *node* set  $\mathcal{V}$  primarily consists of action nodes  $v_{(a,m,s)}$ , each corresponding to an action  $a$  of a microbatch  $m$  at a stage  $s$ , where the action is defined as a combination of

$$a \in \{f, b\}, \quad m \in \{1, \dots, M\}, \quad s \in \{1, \dots, S\}.$$

Here,  $a = f$  and  $a = b$  denote forward and backward computations, respectively, while  $M$  and  $S$  denote the total numbers of microbatches and pipeline stages. In addition, we introduce a source node  $v_s$  and a destination node  $v_d$ , which represent the start and the end of a batch, respectively.

**Pipeline DAG Edges.** Let  $\mathcal{E}$  denote the set of directed edges in the DAG  $\mathcal{G} = (\mathcal{V}, \mathcal{E})$ . Each edge  $v_i \rightarrow v_j \in \mathcal{E}$  represents an execution dependency, indicating that a node  $v_j$  cannot begin until a node  $v_i$  finishes.  $\mathcal{E}$  encodes all necessary intra- and inter-stage execution constraints of the pipeline. The edge construction rules are provided in Appendix B.

**Node Weights.** Each action node  $v_i \in \mathcal{V}$  is associated with a *weight*  $w_i$ , denoting the execution duration of the action,

$$w_i \in [w_i^{\min}, w_i^{\max}], \quad (3)$$

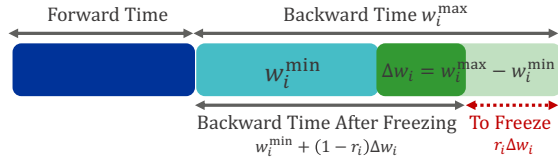


Figure 3. Backward-time reduction via parameter freezing.

where  $w_i^{\min}$  and  $w_i^{\max}$  denote the execution duration when all parameters are frozen and when no parameters are frozen, respectively, as obtained from the monitoring phase. Additionally, for the source and destination nodes, we define  $w_s = w_d = 0$ , since they are abstract nodes that are not associated with any computation.

Figure 3 illustrates how the node weight  $w_i$  varies with the freeze ratio. The execution time of forward actions (blue) remains unchanged, as forward computations are not affected by parameter freezing. Accordingly, for any forward nodes  $i = (f, m, s)$ ,  $w_i = w_i^{\min} = w_i^{\max}$  holds. In contrast, backward actions are affected by parameter freezing. Following the decomposition of backward computation in ZeroBubble analysis (Qi et al., 2023), the backward pass consists of two components: (1) gradient computation with respect to input activations (in cyan in Figure 3) and (2) gradient computation with respect to parameters (in green). Only the latter is influenced by parameter freezing. As a result, even when parameters are fully frozen, the activation-gradient component remains at  $w_i^{\min}$ , while the parameter-gradient component decreases according to the freeze ratio.

**Freeze Ratio.** The *freeze ratio* of a node  $v_i$  is defined as

$$r_i := 1 - \frac{w_i - w_i^{\min}}{w_i^{\max} - w_i^{\min}}, \quad r_i \in [0, 1] \quad (4)$$

when  $w_i^{\max} > w_i^{\min}$ , and we set  $r_i = 0$  when  $w_i^{\max} = w_i^{\min}$ .

Here,  $r_i$  quantifies the average fraction of parameters frozen in a node  $v_i$ . In particular, for forward actions  $v_{(f,m,s)}$

whose execution time does not vary with freezing,

$$w_{(f,m,s)} = w_{(f,m,s)}^{\min} = w_{(f,m,s)}^{\max} \implies r_{(f,m,s)} = 0.$$

**Start Time of Action.** The *start time*  $P_i$  of an action node  $v_i$  is determined by the longest-path over all its predecessors in the DAG such that

$$P_i := \max_{(v_j \rightarrow v_i) \in \mathcal{E}} (P_j + w_j), \quad (5)$$

where the batch start time according to the source node  $v_s$  is defined as  $P_s = 0$ , and the batch execution time corresponds to the start time of the destination node,  $P_d$ .

### 3.2.2. LINEAR PROGRAMMING FORMULATION

We formulate the problem of determining the freeze ratios  $\mathbf{r}$  as a linear program (LP) on the previously defined pipeline DAG. Applying the resulting expected freeze ratios  $\mathbf{r}^*$  selectively shortens backward computations that are related to the critical path of the end-to-end batch execution time. Consequently, the overall batch latency is reduced from  $P_d^{\max}$  (i.e.,  $P_d$  where all  $w_i = w_i^{\max}$ ) to  $P_d^*$ .

**Decision Variables.** For each node  $v_i \in \mathcal{V}$ , including the source and destination nodes  $v_s$  and  $v_d$ , we introduce two non-negative real-valued decision variables:  $P_i \in \mathbb{R}_{\geq 0}$  and  $w_i \in \mathbb{R}_{\geq 0}$ , denoting the start time and duration of a node  $v_i$ , respectively. Together, these variables define the temporal placement of each action block within the pipeline schedule.

**Objective Function.** The objective is twofold: (1) to minimize the batch completion time  $P_d$  as the *primary objective*, and (2) to avoid excessive freezing by minimizing the freeze ratios  $r_i$  as a *secondary objective*, subject to an upper-bound  $r_{\max}$ . We enforce this priority by assigning a sufficiently small  $\lambda \ll 1$  to the secondary goal, so that minimizing  $P_d$  always dominates the optimization. Accordingly, we formulate the linear objective as

$$\min \left[ P_d - \lambda \sum_{i \in \mathcal{V}} \delta_i w_i \right], \quad \lambda \ll 1. \quad (6)$$

The second term therefore acts only as a tie-breaker among solutions with similar batch time  $P_d$ . Here,  $\delta_i$  denotes the reciprocal of the execution-time range, defined as

$$\delta_i = \frac{1}{w_i^{\max} - w_i^{\min}} \quad \text{if } w_i^{\max} > w_i^{\min}, \text{ and } 0 \text{ otherwise.} \quad (7)$$

With this definition, the term  $-\delta_i w_i$  is linearly proportional to the freeze ratio  $r_i$  for freezable nodes, whereas  $\delta_i = 0$  for nodes whose execution time is unaffected by freezing.

**Constraints.** The optimization is subject to the following linear constraints.

- [1]  $P_j \geq P_i + w_i, \quad \forall (i \rightarrow j) \in \mathcal{E},$
- [2]  $w_i^{\min} \leq w_i \leq w_i^{\max}, \quad \forall i \in \mathcal{V},$
- [3]  $P_s = 0, \quad w_s = 0,$
- [4]  $\sum_{i \in \mathcal{V}_s} \delta_i (w_i^{\max} - w_i) \leq r_{\max} |\mathcal{V}_s|, \quad \forall s \in \{1, \dots, S\}.$

Constraint [1] enforces precedence in the DAG, ensuring that an action  $j$  cannot start until all predecessor actions  $i$  have finished. Constraint [2] bounds each action duration within  $[w_i^{\min}, w_i^{\max}]$ , capturing the feasible latency range under parameter freezing. Constraint [3] anchors the beginning of the schedule by setting the source node to  $P_s = w_s = 0$ .

Finally, Constraint [4] imposes a stage-wise *average freezing budget*. Using the linearized freeze ratio  $r_i = \delta_i (w_i^{\max} - w_i)$  (see Equation 4) for freezable backward nodes  $i \in \mathcal{V}_s$  at a stage  $s$ , Constraint [4] is equivalent to

$$\frac{1}{|\mathcal{V}_s|} \sum_{i \in \mathcal{V}_s} r_i \leq r_{\max}, \quad \forall s, \quad (8)$$

which prevents any pipeline stage from being over-frozen on average. Here, let  $\mathcal{V}_s \subseteq \mathcal{V}$  be the set of action nodes assigned to a stage  $s$ , and  $r_{\max}$  be a user-specified *maximum freeze ratio*. Although the constraint is imposed at the stage level,  $r_{\max}$  effectively bounds the expected parameter-level freeze ratio, since each stage is associated with a distinct set of parameters, and parameter freezing is applied via random selection within each action. As a result, this constraint ensures that no parameter exceeds the allowable freeze budget in expectation while preserving the full linearity of the LP.

Solving this LP yields execution times  $w_i$  for all nodes  $v_i \in \mathcal{V}$ , from which freeze ratios  $r_i$  are derived. This formulation ensures that each batch completes in minimal time while freezing parameters in a controlled manner across stages. Moreover, since the formulation imposes no integrality constraints on the variables, it can be solved in polynomial time using standard linear programming solvers, such as interior-point methods (Karmarkar, 1984).

### 3.3. Phase III: Freezing

After determining the expected freeze ratios  $\mathbf{r}^*$ , TimelyFreeze applies freezing in a *progressive* manner. Specifically, the freeze ratio for each action  $v_i$  is gradually increased from zero toward  $r_i^*$ . This smooth transition avoids abrupt changes in freezing behavior that could harm training stability. Formally, at each step  $t$ , parameters are frozen according to the actual freeze ratio  $\text{AFR}_{i,t}$ . Once  $t > T_f$ , the system enters a *stable freezing phase*, where  $\text{AFR}_{i,t} = r_i$ . The actual freeze ratio for  $t > T_m$  is defined as

$$\text{AFR}_{i,t} = \min \left\{ r_i, r_i \cdot \frac{t - T_m}{T_f - T_m} \right\}. \quad (9)$$

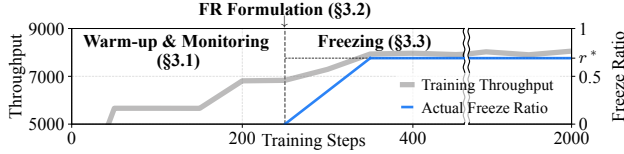


Figure 4. Freeze ratio and training throughput (tokens/sec) across training steps. After warm-up and monitoring, the freeze ratio is gradually increased toward the expected value  $r^*$ , resulting in a corresponding increase in training throughput.

Regarding which parameters to freeze, TimelyFreeze adopts *uniform random selection* as a strong and unbiased reference. Under a given  $AFR_{i,t}$ , this strategy assigns equal freezing probability to all parameters associated with each action. As a result, it isolates the effect of the freeze ratio itself from additional heuristics or parameter-level statistics.

Figure 4 illustrates the evolution of the actual freeze ratio (blue line) over training steps. The actual freeze ratio starts from zero at  $T_m$ , the boundary between the monitoring and freezing phases, and gradually increases toward the expected freeze ratio  $r^*$ . As the actual freeze ratio increases, the training throughput (gray line) improves accordingly. The full step-level algorithm is provided in Appendix C.1.

### 3.4. Time-to-Accuracy Analysis

We analyze convergence in terms of *time-to-accuracy* (TTA), defined as the wall-clock time required to reach an  $\varepsilon$ -stationary point. Formally, TTA is given by

$$TTA = \sum_{t=1}^{T_\varepsilon} \tau_t, \quad (10)$$

where  $T_\varepsilon$  denotes the number of optimization steps required to reach the target stationary level  $\varepsilon$ , and  $\tau_t$  denotes the average execution time at step  $t$ .

**Iteration Complexity.** Compared to the no-freezing baseline, TimelyFreeze may require more optimization steps, since parameter freezing partially suppresses gradient updates. Our analysis makes this trade-off explicit. In expectation, the effective descent per step is reduced proportionally to the fraction of parameters being updated, which yields the iteration-complexity scaling,

$$T_\varepsilon^{\text{ours}} \approx \frac{1}{\bar{p}_{\text{eff}}} T_\varepsilon^{\text{base}}, \quad (11)$$

where  $\bar{p}_{\text{eff}} \in [1 - r_{\max}, 1]$  denotes the average effective update probability (see Appendix D.1 for the definition).

**Per-step Execution Time.** Despite the increase in iteration count, TimelyFreeze reduces the per-step execution time by freezing throughput bottlenecks along the pipeline critical path. We summarize this effect by

$$\tau^{\text{ours}} = \kappa \tau^{\text{base}}, \quad \kappa \in (0, 1), \quad (12)$$

where  $\kappa$  captures the per-step speedup induced by parameter freezing under TimelyFreeze. We note that  $\kappa$  is directly observable in practice. Since  $\tau \propto 1 / \text{throughput}$ , it can be computed from the measured throughput values reported in the experimental results.

**Time-to-Accuracy Trade-off.** Combining the above results, the overall TTA ratio satisfies

$$\frac{TTA_\varepsilon^{\text{ours}}}{TTA_\varepsilon^{\text{base}}} \approx \frac{\kappa}{\bar{p}_{\text{eff}}}. \quad (13)$$

Therefore, TimelyFreeze achieves a smaller time-to-accuracy whenever the per-step speedup outweighs the increase in iteration complexity, i.e.,  $\kappa < \bar{p}_{\text{eff}}$ , which depends on the effective update probability in practice, even for a large  $r_{\max}$ . A detailed derivation is provided in Appendix D.

## 4. Experiments

### 4.1. Hybrid Variants

As discussed in Section 2.3, both baselines, APF (Chen et al., 2023) and AutoFreeze (Liu et al., 2021), jointly determine *how many parameters to freeze* and *which parameters to freeze*, based on gradient-derived metrics.

In contrast, our method focuses solely on the first component by computing stage-wise freeze ratios via our LP formulation, while remaining agnostic to parameter selection. To demonstrate that our method is complementary to existing parameter selection heuristics, we introduce two hybrid variants, TimelyFreeze+APF and TimelyFreeze+Auto. In these variants, TimelyFreeze determines the freeze budget, while APF or AutoFreeze provides the parameter selection metric. Detailed hybrid mechanism is provided in Appendix C.2.

### 4.2. Experimental Setup

**Models and Datasets.** We conduct instruction finetuning task on the LLaMA-3.2-1B, LLaMA-3-8B (Dubey et al., 2023), and LLaMA-2-13B (Touvron et al., 2024) models using the Alpaca-GPT4 (Peng et al., 2023) and OpenHermes-2.5 (Teknium, 2023) datasets to evaluate various freezing methods. To further demonstrate the applicability across domains, we conduct image classification by finetuning pretrained ViT-L/32 (Huggingface, 2025) and ConvNeXt-V2-L (Woo et al., 2023) models on ImageNet-1K (Deng et al., 2009) and Food-101 (Bossard et al., 2014) datasets, respectively. For detailed experiment setup, refer to Appendix E.1. The source code is available at <https://anonymous.4open.science/r/TimelyFreeze/>.

**Pipeline Schedules.** We validate our method under four representative pipeline schedules: *GPipe* (Huang et al., 2019), *IF1B* (Fan et al., 2021), *Interleaved IF1B* (Narayanan et al.,

Table 1. Comparison of freezing methods across different pipeline schedules (LLaMA-3-8B). The average accuracy of the pretrained (no fine-tuning) baseline is 50.81. The best and second-best values among the five freezing methods (APF, AutoFreeze, TimelyFreeze, and two hybrid variants) are highlighted in bold and underline, respectively.  $r_{max}$  for TimelyFreeze is set to 0.8 for all experiments.

GPipe					1F1B					
Freeze Method	Accuracy Preservation		Time Efficiency			Freeze Method	Accuracy Preservation		Time Efficiency	
	Avg. Acc. ( $\Delta$ ) $\uparrow$	Frz. Ratio	Throughput ( $\Delta$ ) $\uparrow$	MFU $\uparrow$	Avg. Acc. ( $\Delta$ ) $\uparrow$	Frz. Ratio	Throughput ( $\Delta$ ) $\uparrow$	MFU $\uparrow$		
No Freezing	54.63 (+0.00)	0.00	5737 (0.00)	25.94	54.63 (+0.00)	0.00	5748 (0.00)	25.99		
APF	<b>54.65 (+0.02)</b>	28.85	7293 ( <b>27.12</b> )	33.20	<b>54.65 (+0.02)</b>	28.85	7312 ( <b>27.20</b> )	33.29		
AutoFreeze	53.99 ( <b>-0.64</b> )	41.69	7351 ( <b>28.13</b> )	33.45	53.99 ( <b>-0.64</b> )	41.69	7367 ( <b>28.15</b> )	33.52		
TimelyFreeze	<u>54.79 (+0.17)</u>	35.64	<u>7821 (36.33)</u>	<u>35.69</u>	54.69 (+0.07)	33.14	<u>7867 (36.87)</u>	<u>35.89</u>		
+APF	<b>54.82 (+0.19)</b>	35.66	<b>7839 (36.63)</b>	<b>35.77</b>	<b>54.84 (+0.21)</b>	34.23	<b>8024 (39.59)</b>	<b>36.66</b>		
+AutoFreeze	54.65 (+0.03)	35.06	7774 ( <b>35.50</b> )	35.44	<u>54.82 (+0.19)</u>	32.62	7827 ( <b>36.16</b> )	35.70		
Interleaved 1F1B										
Freeze Method	Accuracy Preservation		Time Efficiency			Freeze Method	Accuracy Preservation		Time Efficiency	
	Avg. Acc. ( $\Delta$ ) $\uparrow$	Frz. Ratio	Throughput ( $\Delta$ ) $\uparrow$	MFU $\uparrow$			Avg. Acc. ( $\Delta$ ) $\uparrow$	Frz. Ratio	Throughput ( $\Delta$ ) $\uparrow$	MFU $\uparrow$
No Freezing	54.78 (+0.00)	0.00	6173 (0.00)	27.91		No Freezing	54.66 (+0.00)	0.00	6889 (0.00)	31.16
APF	<b>54.99 (+0.21)</b>	58.05	7734 ( <b>25.29</b> )	35.20		APF	54.47 ( <b>-0.19</b> )	43.35	8522 ( <b>23.70</b> )	38.71
AutoFreeze	54.54 ( <b>-0.24</b> )	76.86	7495 ( <b>21.43</b> )	34.10		AutoFreeze	54.86 (+0.20)	24.28	7139 ( <b>3.62</b> )	32.28
TimelyFreeze	54.64 ( <b>-0.14</b> )	60.07	<u>8081 (30.91)</u>	36.78		TimelyFreeze	54.72 (+0.06)	69.92	<b>8939 (29.75)</b>	<b>40.70</b>
+APF	54.71 ( <b>-0.06</b> )	60.72	<b>8108 (31.36)</b>	<b>36.92</b>		+APF	<u>55.03 (+0.37)</u>	69.97	<u>8923 (29.51)</u>	<u>40.63</u>
+AutoFreeze	<u>54.72 (-0.06)</u>	60.76	8057 ( <b>30.53</b> )	36.67		+AutoFreeze	<b>55.05 (+0.39)</b>	70.03	8909 ( <b>29.32</b> )	40.56
ZBV										
Freeze Method	Accuracy Preservation		Time Efficiency			Freeze Method	Accuracy Preservation		Time Efficiency	
	Avg. Acc. ( $\Delta$ ) $\uparrow$	Frz. Ratio	Throughput ( $\Delta$ ) $\uparrow$	MFU $\uparrow$			Avg. Acc. ( $\Delta$ ) $\uparrow$	Frz. Ratio	Throughput ( $\Delta$ ) $\uparrow$	MFU $\uparrow$
No Freezing	54.66 (+0.00)	0.00	6889 (0.00)	31.16		No Freezing	54.66 (+0.00)	0.00	6889 (0.00)	31.16
APF	54.47 ( <b>-0.19</b> )	43.35	8522 ( <b>23.70</b> )	38.71		APF	54.47 ( <b>-0.19</b> )	43.35	8522 ( <b>23.70</b> )	38.71
AutoFreeze	54.86 (+0.20)	24.28	7139 ( <b>3.62</b> )	32.28		AutoFreeze	54.86 (+0.20)	24.28	7139 ( <b>3.62</b> )	32.28
TimelyFreeze	54.72 (+0.06)	69.92	<b>8939 (29.75)</b>	<b>40.70</b>		TimelyFreeze	54.72 (+0.06)	69.92	<b>8939 (29.75)</b>	<b>40.70</b>
+APF	<u>55.03 (+0.37)</u>	69.97	<u>8923 (29.51)</u>	<u>40.63</u>		+APF	<u>55.03 (+0.37)</u>	69.97	<u>8923 (29.51)</u>	<u>40.63</u>
+AutoFreeze	<b>55.05 (+0.39)</b>	70.03	8909 ( <b>29.32</b> )	40.56		+AutoFreeze	<b>55.05 (+0.39)</b>	70.03	8909 ( <b>29.32</b> )	40.56

2021), and *Zero-Bubble V-shaped* (ZBV) (Qi et al., 2023). We employ the TorchTitan framework (Liang et al., 2025) developed by PyTorch team for distributed training.

**Hardware Settings.** All experiments were conducted on four Nvidia A6000 48GB GPUs and four H200 140GB GPUs. A6000 GPUs communicate via PCIe, whereas H200 GPUs communicate through NVLink.

**Metrics.** Model performance is assessed using the *average accuracy* over four widely used benchmarks: *MMLU* (5 shots) (Hendrycks et al., 2020), *HellaSwag* (zero shot) (Zellers et al., 2019), *ARC-Challenge* (ARC-C) (10 shots) (Clark et al., 2018), and *TruthfulQA* (zero shot) (Lin et al., 2022). We report the mean proportion of frozen parameters across all GPUs using the *average freeze ratio* (“Frz. Ratio” in Table 1), which is defined as

$$\text{Average Freeze Ratio} := \mathbb{E}_{t,i,j} \left[ \mathbb{I}_{t,i}^{(j)} \right],$$

where  $\mathbb{I}_{t,i}^{(j)}$  is a Bernoulli random variable induced by uniform random freezing, indicating whether a parameter  $j$  of node  $v_i$  is frozen at step  $t$ .

## 5. Results and Discussion

Table 1 shows the accuracy preservation and time efficiency results for LLaMA-3-8B under four pipeline schedules. Here, the accuracy gain (e.g.,  $\Delta$  of Avg. Acc.) denotes the difference in average accuracy relative to the no-freezing baseline, while throughput gain ( $\Delta$  of Throughput) represents the relative throughput improvement.

Across all pipeline schedules, TimelyFreeze and its hybrids consistently improve throughput over the no-freezing baseline, while largely preserving accuracy. In particular, under the 1F1B schedule, TimelyFreeze+APF achieves the highest throughput improvement of 39.59% with comparable accuracy, and in some cases slightly surpasses the no-freezing baseline. Compared to the baseline freezing methods (APF and AutoFreeze), TimelyFreeze and its hybrids generally achieve higher or comparable accuracy across the GPipe, 1F1B, and ZBV schedules.

### 5.1. Scaling Toward Larger Models

Figure 5 presents the accuracy–throughput trade-offs for the LLaMA family as the model size scales from 1B to 8B and 13B under four pipeline schedules. Across most settings, TimelyFreeze and its hybrid variants consistently lie on or near the Pareto frontier, achieving higher throughput with comparable accuracy relative to both the no-freezing baseline and baseline freezing methods.

For LLaMA-1B (top) in Figure 5, TimelyFreeze and its hybrids achieve moderate throughput improvements of up to 19–21% with less than 1%p accuracy degradation compared to the no-freezing baseline.

As the model size increases, these gains become more pronounced. On LLaMA-8B (middle) and LLaMA-13B (bottom), TimelyFreeze yields substantially larger throughput improvements across GPipe and 1F1B schedules, even up to 46% than the no-freezing baseline in 13B, while preserving accuracy at the comparable extent. For In-

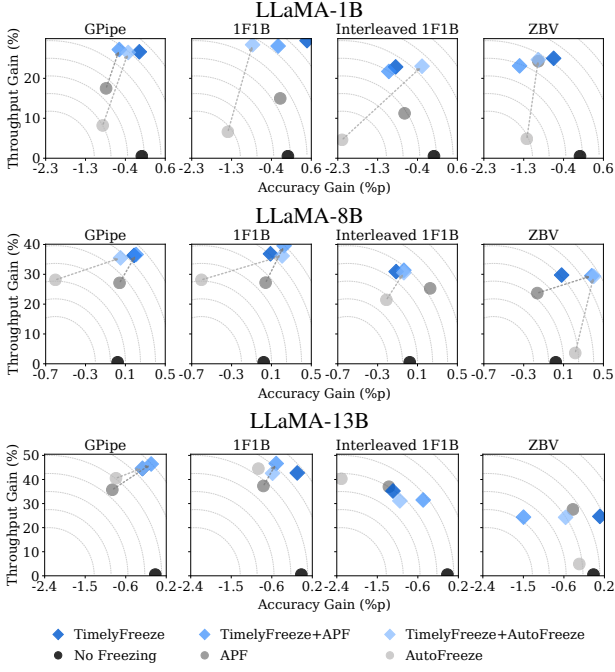


Figure 5. Comparison of accuracy–throughput trade-offs under GPipe, 1F1B, Interleaved 1F1B, and Zero-Bubble (ZBV).

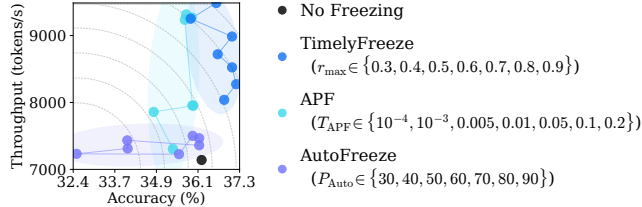


Figure 6. Accuracy–throughput trade-offs on LLaMA-1B under different freezing controller values with the 1F1B schedule.

terleaved 1F1B and ZBV on LLaMA-13B, accuracy shows higher variance, suggesting that additional multi-seed evaluation would be useful to assess stability at this scale.

Overall, the scaling results indicate that TimelyFreeze scales favorably with model size, yielding higher throughput gains while maintaining comparable accuracy. See Appendices E.2–E.3 for the detailed numbers and benchmark scores. In addition, the examples of actual pipeline execution schedules are visualized in Appendix F.1.

## 5.2. Freezing Controller Sensitivity

In Figure 6, we analyze the accuracy–throughput trade-off of the LLaMA-1B model across different user-specified freezing controller values (i.e.,  $r_{\max}$  for TimelyFreeze,  $T_{\text{APF}}$  for APF, and  $P_{\text{Auto}}$  for AutoFreeze). The control values used for each method are indicated in the figure, and the corresponding results are arranged from left to right in the order of increasing freezing strength.

TimelyFreeze exhibits a consistent trend, as  $r_{\max}$  decreases (i.e., weaker freezing), throughput decreases monotonically while accuracy remains well preserved across different  $r_{\max}$  values. In contrast, the two baselines consistently achieve lower throughput and accuracy than TimelyFreeze across all controller settings. Moreover, their throughput and accuracy vary irregularly as the user-specified hyperparameters change, indicating that  $r_{\max}$  provides more predictable and controllable throughput behavior in TimelyFreeze. Based on our experience, we recommend selecting  $r_{\max}$  in the range of [0.5, 0.8], where accuracy is rather stable, depending on the desired accuracy–throughput trade-off.

## 5.3. Generalization on Vision Models

We further evaluate the generality of TimelyFreeze on vision models, including ViT-L/32 and ConvNeXt-V2-L, with detailed results reported in Appendix G.

ConvNeXt-V2-L exhibits highly unbalanced parameter distributions, where deeper layers contain substantially larger parameter groups, leading to execution-time skew under pipeline parallelism. As explained in Appendix G.1, across different partitioning heuristics, TimelyFreeze consistently reduces training time while maintaining accuracy comparable to existing freezing methods. Under the GPipe and 1F1B schedules, TimelyFreeze often attains the best or second-best training time among all freezing methods, despite using moderate freeze ratios. This result shows that LP-based, pipeline-aware freezing effectively addresses execution-time imbalance arising from architectural unevenness.

Consistent robustness is also observed for ViT-L/32 finetuning in Appendix G.2. While APF suffers from severe accuracy degradation due to aggressive, metric-driven freezing, TimelyFreeze preserves accuracy close to the no-freezing baseline while achieving the largest training-time reduction under both pipeline schedules. This result indicates that TimelyFreeze generalizes robustly beyond a specific model structure or task, providing stable performance even when importance metrics are noisy or unreliable.

## 6. Conclusion

We proposed **TimelyFreeze**, an adaptive parameter-freezing mechanism for pipeline-parallel training that explicitly incorporates pipeline execution structure. By modeling the pipeline schedule as a DAG and computing stage-wise freeze ratios via linear programming, TimelyFreeze reduces batch latency while preserving model accuracy. Extensive experiments on large language models and vision models demonstrate that TimelyFreeze consistently achieves superior accuracy–throughput trade-offs across pipeline schedules. Future work includes extending TimelyFreeze to multi-node settings and integrating it with hybrid parallelism.

## Acknowledgements

This work was supported by Institute of Information & Communications Technology Planning & Evaluation (IITP) grant funded by the Korea government (MSIT) (No. RS-2020-II200862, DB4DL: High-Usability and Performance In-Memory Distributed DBMS for Deep Learning, 50% and No. RS-2022-II220157, Robust, Fair, Extensible Data-Centric Continual Learning, 50%).

## Impact Statement

This work introduces TimelyFreeze, a system-level optimization technique that improves the efficiency of pipeline-parallel training by aligning parameter-freezing decisions with execution-time dynamics. By reducing redundant computation without modifying model architectures or learning objectives, TimelyFreeze can lower training time and computational cost for large-scale models, potentially reducing energy consumption and improving accessibility to large-model training in resource-constrained environments.

The method is intended for use in controlled training settings and does not alter model inference behavior or introduce new capabilities that could raise additional ethical concerns beyond those associated with the underlying models. As with other efficiency-oriented system optimizations, the broader societal impacts of this work depend on how large-scale models are ultimately deployed. Overall, we do not foresee any specific negative impacts unique to TimelyFreeze beyond those already present in large-scale model training and deployment.

## References

Bossard, L., Guillaumin, M., and Van Gool, L. Food-101 – mining discriminative components with random forests. In *Proceedings of the European Conference on Computer Vision*, pp. 446–461, 2014.

Brock, A., Lim, T., Ritchie, J. M., and Weston, N. Freeze-out: Accelerate training by progressively freezing layers. *arXiv preprint arXiv:1706.04983*, 2017.

Chen, C., Xu, H., Wang, W., Li, B., Li, B., Chen, L., and Zhang, G. Synchronize only the immature parameters: Communication-efficient federated learning by freezing parameters adaptively. *IEEE Transactions on Parallel and Distributed Systems*, 35(7):1155–1173, 2023.

Clark, P., Cowhey, I., Etzioni, O., Khot, T., Sabharwal, A., Schoenick, C., and Tafjord, O. Think you have solved question answering? try arc, the ai2 reasoning challenge. *arXiv preprint arXiv:1803.05457*, 2018.

Deng, J., Dong, W., Socher, R., Li, L.-J., Li, K., and Fei-Fei, L. ImageNet: A large-scale hierarchical image database. In *Proceedings of the IEEE/CVF Conference on Computer Vision and Pattern Recognition*, pp. 248–255, 2009.

Dubey, A., Jauhri, A., Pandey, A., Kadian, A., Al-Dahle, A., Letman, A., Mathur, A., Schelten, A., Yang, A., Fan, A., et al. Llama 2: Open foundation and fine-tuned chat models. *arXiv preprint arXiv:2307.09288*, 2023.

Fan, S., Rong, Y., Meng, C., Cao, Z., Wang, S., Zheng, Z., Wu, C., Long, G., Yang, J., Xia, L., et al. Dapple: A pipelined data parallel approach for training large models. In *Proceedings of the ACM SIGPLAN Symposium on Principles and Practice of Parallel Programming*, pp. 431–445, 2021.

He, C., Li, S., Soltanolkotabi, M., and Avestimehr, S. Pipetransformer: Automated elastic pipelining for distributed training of large-scale models. In *Proceedings of the International Conference on Machine Learning*, pp. 4150–4159. PMLR, 2021.

Hendrycks, D., Burns, C., Basart, S., Zou, A., Mazeika, M., Song, D., and Steinhardt, J. Measuring massive multitask language understanding. *arXiv preprint arXiv:2009.03300*, 2020.

Huang, Y., Cheng, Y., Bapna, A., Firat, O., Chen, D., Chen, M., Lee, H., Ngiam, J., Le, Q. V., Wu, Y., et al. Gpipe: Efficient training of giant neural networks using pipeline parallelism. In *Proceedings of the International Conference on Machine Learning*, pp. 103–112, 2019.

Huggingface. Vision transformer (vit), 2025. URL [https://huggingface.co/docs/transformers/model\\_doc/vit](https://huggingface.co/docs/transformers/model_doc/vit).

Kaplan, J., McCandlish, S., Henighan, T., Brown, T. B., Chess, B., Child, R., Gray, S., Radford, A., Wu, J., and Amodei, D. Scaling laws for neural language models. In *arXiv.org*, 2020.

Karmarkar, N. A new polynomial-time algorithm for linear programming. *Combinatorica*, 4(4):373–395, 1984. doi: 10.1007/BF02579150.

Lee, J., Tang, R., and Lin, J. What would elsa do? freezing layers during transformer fine-tuning. *arXiv preprint arXiv:1911.03090*, 2019.

Li, S., Yuan, G., Dai, Y., Zhang, Y., Wang, Y., and Tang, X. Smartfrz: An efficient training framework using attention-based layer freezing. *arXiv preprint arXiv:2401.16720*, 2024.

Liang, W., Liu, T., Wright, L., Constable, W., Gu, A., Huang, C.-C., Zhang, I., Feng, W., Huang, H., Wang, J., et al. Torch titan: One-stop pytorch native solution for production ready LLM pretraining. In *Proceedings of the International Conference on Learning Representations*, 2025.

Lin, S., Hilton, J., and Evans, O. Truthfulqa: Measuring how models mimic human falsehoods. In *Proceedings of the Annual Meeting of the Association for Computational Linguistics*, pp. 3214–3252, 2022.

Liu, Y., Agarwal, S., and Venkataraman, S. Autofreeze: Automatically freezing model blocks to accelerate fine-tuning. *arXiv preprint arXiv:2102.01386*, 2021.

Narayanan, D., Harlap, A., Phanishayee, A., Seshadri, V., Devanur, N. R., Ganger, G. R., Gibbons, P. B., and Zaharia, M. Pipedream: Generalized pipeline parallelism for DNN training. In *Proceedings of the ACM Symposium on Operating Systems Principles*, pp. 1–15, 2019.

Narayanan, D., Shoeybi, M., Casper, J., LeGresley, P., Patwary, M., Korthikanti, V., Vainbrand, D., Kashinkunti, P., Bernauer, J., Catanzaro, B., et al. Efficient large-scale language model training on GPU clusters using megatron-LM. In *Proceedings of the International Conference for High Performance Computing, Networking, Storage and Analysis*, pp. 1–15, 2021.

Peng, B., Li, C., He, P., Galley, M., and Gao, J. Instruction tuning with gpt-4. *arXiv preprint arXiv:2304.03277*, 2023.

Qi, P., Wan, X., Huang, G., and Lin, M. Zero bubble pipeline parallelism. *arXiv preprint arXiv:2401.10241*, 2023.

Qi, P., Wan, X., Amar, N., and Lin, M. Pipeline parallelism with controllable memory. *arXiv preprint arXiv:2405.15362*, 2024.

Sergeev, A. and Del Balso, M. Horovod: Fast and easy distributed deep learning in tensorflow. *arXiv preprint arXiv:1802.05799*, 2018.

Shoeybi, M., Patwary, M., Puri, R., LeGresley, P., Casper, J., and Catanzaro, B. Megatron-LM: Training multi-billion parameter language models using model parallelism. *arXiv preprint arXiv:1909.08053*, 2019.

Teknium. Openhermes 2.5: An open dataset of synthetic data for generalist llm assistants, 2023. URL <https://huggingface.co/datasets/teknium/OpenHermes-2.5>.

Touvron, H., Martin, L., Stone, K., Albert, P., Almahairi, A., Babaei, Y., Bashlykov, N., Batra, S., Bhargava, P., et al. The Llama 3 herd of models. *arXiv preprint arXiv:2407.21783*, 2024.

Wang, Y., Sun, D., Chen, K., Lai, F., and Chowdhury, M. Egeria: Efficient DNN training with knowledge-guided layer freezing. In *Proceedings of the European Conference on Computer Systems*, pp. 851–866, 2023.

Woo, S., Debnath, S., Hu, R., Chen, X., Liu, Z., Kweon, I. S., and Xie, S. Convnext v2: Co-designing and scaling convnets with masked autoencoders. In *Proceedings of the IEEE/CVF Conference on Computer Vision and Pattern Recognition*, pp. 16133–16142, 2023.

You, Y., Zhang, Z., Hsieh, C.-J., Demmel, J., and Keutzer, K. Imagenet training in minutes. In *Proceedings of the International Conference on Parallel Processing*, pp. 1–10, 2018.

Zellers, R., Holtzman, A., Bisk, Y., Farhadi, A., and Choi, Y. Hellaswag: Can a machine really finish your sentence? *arXiv preprint arXiv:1905.07830*, 2019.

## A. Notations

Table 2. Notation used in TimelyFreeze.

Symbol	Description
$\mathcal{G} = (\mathcal{V}, \mathcal{E})$	Directed acyclic graph (DAG) representing a pipeline schedule.
$\mathcal{V}$	Set of action nodes in the pipeline DAG.
$\mathcal{E}$	Set of directed edges encoding precedence constraints.
$v_{(a,m,s)}$	Action node with action type $a$ , microbatch $m$ , at stage $s$ . For simplicity, it is also denoted as $v_i$ .
$a \in \{f, b\}$	Action type: forward ( $f$ ) or backward ( $b$ ).
$m \in \{1, \dots, M\}$	Microbatch index; $M$ is the total number of microbatches.
$s \in \{1, \dots, S\}$	Pipeline stage index; $S$ is the number of stages.
$v_s, v_d$	Source and destination nodes representing batch start and completion.
$P_i$	Start time of action node $v_i$ , determined by the longest path in $\mathcal{G}$ .
$P_d$	Start time of destination node $v_d$ , corresponding to batch execution time.
$w_i$	Execution time (duration) of action node $v_i$ .
$w_i^{\min}, w_i^{\max}$	Minimum and maximum execution times of node $v_i$ under full and no freezing.
$r_i$	Expected freeze ratio of action node $v_i$ .
$r_{\max}$	Maximum average freeze ratio allowed per pipeline stage specified by the user.
$t \in \{1, \dots, T_{\text{tot}}\}$	Training step; $T_{\text{tot}}$ is the total number of training steps.
$T_w, T_m, T_f$	The last step of the warm-up, monitoring, and progressive freezing phase, respectively.
$N$	Total number of model parameters.
$N_s$	Number of parameters in stage $s$ and $N = \sum_{s=1}^S N_s$ holds.
$\mathbb{I}_{t,i}$	Binary freezing mask of the action node $v_i$ at step $t$ ; $\mathbb{I}_{t,i}^{(j)} = 1$ if parameter $j$ associated with $v_i$ is selected to be frozen at step $t$ , and 0 otherwise.

## B. Edge Construction Rules

1. *Source and destination connections:* The source and destination nodes are connected to the actions nodes as

$$v_s \rightarrow v_{(f,1,1)}, \quad v_{(b,M,1)} \rightarrow v_d.$$

Here, a batch starts with the forward action of the first microbatch at the first stage and ends with the backward action of the last microbatch at the first stage.

2. *Intra-stage dependencies:* Within each stage, any action of microbatch  $m + 1$  starts only after the corresponding action of microbatch  $m$  finishes. Moreover, each backward action must follow its corresponding forward action.

$$v_{(a,m,s)} \rightarrow v_{(a,m+1,s)}, \quad v_{(f,m,s)} \rightarrow v_{(b,m,s)}.$$

3. *Inter-stage dependencies:* A forward action at stage  $s + 1$  can begin only after the forward action at stage  $s$  completes, and a backward action at stage  $s - 1$  can begin only after the backward action at stage  $s$  completes.

$$v_{(f,m,s)} \rightarrow v_{(f,m,s+1)}, \quad v_{(b,m,s)} \rightarrow v_{(b,m,s-1)}.$$

4. *Pipeline schedule dependencies:* For action nodes assigned to the same GPU rank, the execution order defined by the pipeline schedule must be respected. This constraint depends on the pipeline schedule. For example, under GPipe, any backward action can begin only after the last forward microbatch completes (i.e.,  $v_{(f,M,s)} \rightarrow v_{(b,1,s)}$ ), whereas 1F1B does not impose this constraint.

## C. Algorithms

### C.1. TimelyFreeze's Freezing Algorithm

---

#### Algorithm 1 Step-Level Freeze Ratio Scheduling (Stage $s$ )

**Input:** Phase boundaries  $\{T_w, T_m, T_f, T_{total}\}$ ; Parameter set  $\mathcal{P}_s$  and action set  $\mathcal{V}_s$  corresponding to stage  $s$ .

---

```

1 for  $t \leftarrow 1$  to  $T_{total}$  do
2   if  $t \leq T_w$  then
3     continue                                ▷ Warm-up (no freezing)
4   foreach  $v_i \in \mathcal{V}_g$  do
5     Record execution time  $\tau_{i,t}$ 
6   if  $T_w < t \leq T_m/2$  then
7     foreach  $v_i$  do
8        $\text{AFR}_{i,t} \leftarrow 0$                   ▷ Upperbound Monitoring
9   else if  $T_m/2 < t \leq T_m$  then
10    foreach  $v_i$  do
11       $\text{AFR}_{i,t} \leftarrow 1$                   ▷ Lowerbound Monitoring
12  else if  $t = T_m$  then
13     $\{\tau\} \leftarrow$  All-gather  $\{\tau_{i,t'} : v_i \in \mathcal{V}_s, t' = 1, \dots, T_m\}$  across stages  $\{s = 1, \dots, S\}$ 
14     $\{r_i\}, \{P_i\} \leftarrow \text{LPSOLVER}(\{\tau\})$           ▷ LP Formulation
15  else
16    foreach  $v_i \in \mathcal{V}_s$  do
17       $\text{AFR}_{i,t} \leftarrow \min \left\{ r_i, r_i \cdot \frac{t - T_m}{T_f - T_m} \right\}$           ▷ Freezing
18      Randomly select  $I_i \subseteq \mathcal{P}_s$  such that  $E[|I_i|] = \text{AFR}_{i,t} \cdot |\mathcal{P}_s|$ 
19      Freeze parameters in  $I_i$ 

```

---

### C.2. Hybrid Variants Algorithm

---

#### Algorithm 2 Metric-Aware Parameter Selection for TimelyFreeze+APF / TimelyFreeze+Auto

**Input:** Expected freeze ratios  $\{r_i\}$  from TimelyFreeze; Current step  $t$  and stage  $s$ ; Number of parameters  $N_s$  in stage  $s$ ; Baseline method's freezing mask  $\mathbb{I}_{base,t}$  at step  $t$ .

**Output:** Binary freezing mask  $\mathbb{I}_t \in \{0, 1\}^{n_s}$

---

```

1 foreach  $v_i \in \mathcal{V}_s$  do
2    $N_{freeze} \leftarrow \lfloor r_i \cdot N_s \rfloor$           ▷ Number of freezing parameters
3   if  $\|\mathbb{I}_{t,i}\|_1 = N_{freeze}$  then
4      $\mathbb{I}_{t,i} \leftarrow \mathbb{I}_{base,t,i}$ 
5   else if  $\|\mathbb{I}_{t,i}\|_1 < N_{freeze}$  then
6      $\mathcal{P}_{add} \leftarrow$  Uniformly sample  $(N_{freeze} - \|\mathbb{I}_{t,i}\|_1)$  indices from  $\{j \mid \mathbb{I}_{t,i}^{(j)} = 0\}$ 
7      $\mathbb{I}_{t,i}^{(j)} \leftarrow \mathbb{I}[\mathbb{I}_{base,t,i}^{(j)} = 1 \vee j \in \mathcal{P}_{add}], \forall j \in \{1, \dots, n_s\}$ 
8   else
9      $\mathcal{P}_{sub} \leftarrow$  Uniformly sample  $(\|\mathbb{I}_{t,i}\|_1 - N_{freeze})$  indices from  $\{j \mid \mathbb{I}_{t,i}^{(j)} = 1\}$ 
10     $\mathbb{I}_{t,i}^{(j)} \leftarrow \mathbb{I}[\mathbb{I}_{base,t,i}^{(j)} = 1 \wedge j \notin \mathcal{P}_{sub}], \forall j \in \{1, \dots, n_s\}$ 
11  Freeze all parameters  $j$  such that  $\mathbb{I}_{t,i}^{(j)} = 1$ 

```

---

## D. Time-to-Accuracy Analysis

In this section, we analyze the *wall-clock time-to-accuracy* (TTA), defined as

$$\text{TTA}_{\varepsilon}^{\text{alg}} := \mathbb{E} \left[ \sum_{t=1}^{T_{\varepsilon}^{\text{alg}}} \tau_t^{\text{alg}} \right]. \quad (14)$$

Here,  $T_{\varepsilon}^{\text{alg}}$  denotes the (sufficient) number of training steps required by freezing algorithm alg to reach a target error  $\varepsilon$  under the specified convergence criterion, and  $\tau_t^{\text{alg}}$  is the execution time of step  $t$  under alg. Accordingly, we decompose the TTA analysis into two components: (1) the iteration complexity  $T_{\varepsilon}^{\text{alg}}$  (Section D.1), and (2) the per-step execution time  $\tau_t^{\text{alg}}$  (Section D.2). Finally, we combine these two results to compare the overall TTA of TimelyFreeze with that of the no-freezing baseline in Section D.3.

### D.1. Convergence Analysis

Under the assumptions in Section D.1.1 and the lemmas in Section D.1.3, we analyze the convergence behavior of a SGD framework under TimelyFreeze and characterize the number of training steps required to reach a target stationary level. Specifically, we derive the iteration complexity under TimelyFreeze (denoted by  $T_{\varepsilon}^{\text{ours}}$ ) in Section D.1.4, and compare it with that of the *no-freezing baseline* ( $T_{\varepsilon}^{\text{base}}$ ) in Section D.1.5.

A training step is indexed by  $t \in \{1, \dots, T\}$ , and each step consists of  $M$  microbatches. For simplicity, we assume that a gradient update is performed after each batch execution, so that the number of training steps coincides with the number of executed batches. Let  $\theta_t \in \mathbb{R}^N$  denote the model parameters at step  $t$ , where  $N$  is the number of trainable parameters, and define the population objective as

$$F(\theta) := \mathbb{E}_{\xi \sim \mathcal{D}} [\ell(\theta; \xi)]. \quad (15)$$

For each microbatch  $m \in \{1, \dots, M\}$ , we define the stochastic gradient

$$g_{t,m} := \nabla_{\theta} \ell(\theta_t; \xi_{t,m}). \quad (16)$$

**Iteration Complexity.** For an algorithm  $\text{alg} \in \{\text{ours}, \text{base}\}$ , we define its *iteration complexity*  $T_{\varepsilon}^{\text{alg}}$  as the smallest number of training steps required to reach an  $\varepsilon$ -stationary point, measured by the expected squared gradient norm, i.e.,

$$T_{\varepsilon}^{\text{alg}} := \inf \left\{ T \in \mathbb{N} : \frac{1}{T} \sum_{t=1}^T \mathbb{E} [\|\nabla F(\theta_t)\|^2] \leq \varepsilon \right\}. \quad (17)$$

**Freezing and Update Masks (Our Convention).** Let  $\mathbb{I}_{t,m} \in \{0, 1\}^N$  denote the *freezing mask* applied at step  $t$  and microbatch  $m$ , where for each parameter  $j \in \{1, \dots, N\}$ ,

$$\mathbb{I}_{t,m}^{(j)} = 1 \text{ indicates that parameter } j \text{ is frozen (no update), } \quad \mathbb{I}_{t,m}^{(j)} = 0 \text{ indicates that parameter } j \text{ is updated.} \quad (18)$$

For convenience, we define the corresponding *update mask* as

$$\mathbb{U}_{t,m}^{(j)} := \mathbf{1} - \mathbb{I}_{t,m}^{(j)} \in \{0, 1\}^N, \quad (19)$$

where  $\mathbb{U}_{t,m}^{(j)} = 1$  indicates that parameter  $j$  is updated and  $\mathbb{U}_{t,m}^{(j)} = 0$  otherwise.

**Update Rule.** The model parameters are updated using masked microbatch gradients as

$$\theta_{t+1} = \theta_t - \eta \Delta_t, \quad \Delta_t := \frac{1}{M} \sum_{m=1}^M (\mathbb{U}_{t,m} \odot g_{t,m}), \quad (20)$$

where  $\eta > 0$  is the stepsize. For simplicity, we assume a constant stepsize  $\eta$  across training steps.

### D.1.1. ASSUMPTIONS

**Assumption D.1** (*L*-Smoothness).  $F$  is  $L$ -smooth:

$$F(y) \leq F(x) + \langle \nabla F(x), y - x \rangle + \frac{L}{2} \|y - x\|^2, \quad \forall x, y. \quad (21)$$

**Assumption D.2** (Unbiased Gradients and Bounded Variance). For all step  $t$  and microbatch  $m$ ,

$$\mathbb{E}[g_{t,m} \mid \theta_t] = \nabla F(\theta_t), \quad \mathbb{E}[\|g_{t,m} - \nabla F(\theta_t)\|^2 \mid \theta_t] \leq \sigma^2. \quad (22)$$

**Assumption D.3** (Conditional Independence of Freezing). Conditioned on  $\theta_t$ , the mask and the stochastic gradient are independent:

$$\mathbb{I}_{t,m} \perp g_{t,m} \mid \theta_t \iff \mathbb{U}_{t,m} \perp g_{t,m} \mid \theta_t. \quad (23)$$

**Assumption D.4** (Bounded Freeze Ratio). Let the per-parameter *update probability* be

$$p_{t,m}^{(j)} := \mathbb{E}[\mathbb{U}_{t,m}^{(j)} \mid \theta_t] = 1 - \mathbb{E}[\mathbb{I}_{t,m}^{(j)} \mid \theta_t]. \quad (24)$$

Assume it is uniformly lower bounded by

$$p_{\min} := 1 - r_{\max} \leq p_{t,m}^{(j)}, \quad \forall t, m, j, \quad (25)$$

where  $r_{\max} \in [0, 1]$  is a user-specified *maximum freeze ratio* as first mentioned in Equation 8.

**Assumption D.5** (Conditional Independence across Microbatches). Conditioned on  $\theta_t$ ,  $\{(\mathbb{I}_{t,m}, g_{t,m})\}_{m=1}^M$  are independent across  $m$ .

### D.1.2. AUXILIARY DEFINITIONS

**Definition D.6** (Average Update Probability).

$$\bar{p}_t := \frac{1}{M} \sum_{m=1}^M p_{t,m}. \quad (26)$$

This quantity averages per-microbatch update probabilities over  $M$  microbatches.

**Definition D.7** (Effective Update Probability). We define the *effective update probability* at step  $t$  as

$$p_{\text{eff},t} := \frac{\sum_{j=1}^N \bar{p}_t^{(j)} (\partial_j F(\theta_t))^2}{\|\nabla F(\theta_t)\|^2}, \quad (27)$$

whenever  $\nabla F(\theta_t) \neq 0$  (and set  $p_{\text{eff},t} := 1$  otherwise). This quantity captures the fraction of gradient energy that is effectively updated under freezing.

**Definition D.8** (Average Effective Update Probability). For a given training horizon  $T$ , we define

$$\bar{p}_{\text{eff}} := \frac{\sum_{t=1}^T \mathbb{E}[p_{\text{eff},t} \|\nabla F(\theta_t)\|^2]}{\sum_{t=1}^T \mathbb{E}[\|\nabla F(\theta_t)\|^2]}. \quad (28)$$

This quantity summarizes the effective update probabilities over the entire training horizon.

### D.1.3. LEMMAS

**Lemma D.9** (Mean of Masked Microbatch Gradient). *Under Assumptions D.2 and D.3, for each  $m$ ,*

$$\mathbb{E}[\mathbb{U}_{t,m} \odot g_{t,m} \mid \theta_t] = \mathbb{E}[\mathbb{U}_{t,m} \mid \theta_t] \odot \mathbb{E}[g_{t,m} \mid \theta_t] = p_{t,m} \odot \nabla F(\theta_t), \quad (29)$$

where  $p_{t,m} \in [0, 1]^N$  stacks  $\{p_{t,m}^{(j)}\}_j$ . Hence, using Equation 20 and Definition D.6,

$$\mathbb{E}[\Delta_t \mid \theta_t] = \bar{p}_t \odot \nabla F(\theta_t). \quad (30)$$

**Lemma D.10** (Descent Inner Product (Worst-case Bound)). *Under Assumptions D.3 and D.4,*

$$\left\langle \nabla F(\theta_t), \mathbb{E}[\Delta_t \mid \theta_t] \right\rangle = \sum_{j=1}^N \bar{p}_t^{(j)} (\partial_j F(\theta_t))^2 \geq p_{\min} \|\nabla F(\theta_t)\|^2. \quad (31)$$

**Lemma D.11** (Descent Inner Product (Exact Characterization)). *Using Definition D.7, we have*

$$\left\langle \nabla F(\theta_t), \mathbb{E}[\Delta_t \mid \theta_t] \right\rangle = p_{\text{eff},t} \|\nabla F(\theta_t)\|^2, \quad (32)$$

and hence  $p_{\text{eff},t} \in [p_{\min}, 1]$ .

**Lemma D.12** (Second Moment of Masked Microbatch Average). *Under Assumptions D.2 and D.5,*

$$\mathbb{E}[\|\Delta_t\|^2 \mid \theta_t] \leq \left(1 + \frac{1}{M}\right) \|\nabla F(\theta_t)\|^2 + \frac{\sigma^2}{M}. \quad (33)$$

*Proof Sketch.* Using the second-moment decomposition  $\mathbb{E}\|X\|^2 = \|\mathbb{E}X\|^2 + \text{Var}(X)$  and Lemma D.9,

$$\|\mathbb{E}[\Delta_t \mid \theta_t]\|^2 = \|\bar{p}_t \odot \nabla F(\theta_t)\|^2 \leq \|\nabla F(\theta_t)\|^2.$$

By conditional independence across  $m$ ,

$$\text{Var}(\Delta_t \mid \theta_t) = \frac{1}{M^2} \sum_{m=1}^M \text{Var}(\mathbb{U}_{t,m} \odot g_{t,m} \mid \theta_t) \leq \frac{1}{M^2} \sum_{m=1}^M \mathbb{E}[\|\mathbb{U}_{t,m} \odot g_{t,m}\|^2 \mid \theta_t].$$

Since  $\mathbb{U}_{t,m}^{(j)} \in \{0, 1\}$ ,  $\|\mathbb{U}_{t,m} \odot g_{t,m}\|^2 \leq \|g_{t,m}\|^2$ , and by Assumption D.2,  $\mathbb{E}\|g_{t,m}\|^2 \leq \|\nabla F(\theta_t)\|^2 + \sigma^2$ . Combining yields Equation 33.

#### D.1.4. ITERATION COMPLEXITY UNDER TIMELYFREEZE

**Theorem D.13** (Iteration Complexity under TimelyFreeze). *Based on Assumptions D.1–D.5, the update rule Equation 20, and Lemmas D.11 and D.12, fix a training horizon  $T \geq 1$  and let  $\bar{p}_{\text{eff}}$  be defined in Definition D.8. If the stepsize satisfies*

$$\eta \leq \frac{p_{\min}}{L(1 + 1/M)} = \frac{1 - r_{\max}}{L(1 + 1/M)}, \quad (34)$$

then

$$\frac{1}{T} \sum_{t=1}^T \mathbb{E}\|\nabla F(\theta_t)\|^2 \leq \frac{2(F(\theta_1) - F^*)}{\bar{p}_{\text{eff}} \eta T} + \frac{L\eta}{\bar{p}_{\text{eff}}} \cdot \frac{\sigma^2}{M}, \quad (35)$$

where  $F^* := \inf_{\theta} F(\theta)$ .

*Proof.* By  $L$ -smoothness Equation 21, for  $x = \theta_t$  and  $y = \theta_{t+1} = \theta_t - \eta \Delta_t$ , we have

$$F(\theta_{t+1}) \leq F(\theta_t) - \eta \langle \nabla F(\theta_t), \Delta_t \rangle + \frac{L\eta^2}{2} \|\Delta_t\|^2.$$

Taking conditional expectation given  $\theta_t$  and applying Lemmas D.11 and D.12 yield

$$\mathbb{E}[F(\theta_{t+1}) \mid \theta_t] \leq F(\theta_t) - \eta p_{\text{eff},t} \|\nabla F(\theta_t)\|^2 + \frac{L\eta^2}{2} \left( \left(1 + \frac{1}{M}\right) \|\nabla F(\theta_t)\|^2 + \frac{\sigma^2}{M} \right).$$

Under the stepsize condition Equation 34 and since  $p_{\text{eff},t} \geq p_{\min}$  for all  $t$ , we have

$$\eta p_{\text{eff},t} - \frac{L\eta^2}{2} \left(1 + \frac{1}{M}\right) \geq \frac{\eta p_{\text{eff},t}}{2}.$$

Therefore,

$$\mathbb{E}[F(\theta_{t+1})] \leq \mathbb{E}[F(\theta_t)] - \frac{\eta}{2} \mathbb{E}[p_{\text{eff},t} \|\nabla F(\theta_t)\|^2] + \frac{L\eta^2}{2} \cdot \frac{\sigma^2}{M}.$$

Summing over  $t = 1, \dots, T$  and using  $F(\theta_{T+1}) \geq F^*$  give

$$\frac{\eta}{2} \sum_{t=1}^T \mathbb{E}[p_{\text{eff},t} \|\nabla F(\theta_t)\|^2] \leq F(\theta_1) - F^* + \frac{L\eta^2}{2} \cdot \frac{\sigma^2}{M} T.$$

By Definition D.8,

$$\sum_{t=1}^T \mathbb{E}[p_{\text{eff},t} \|\nabla F(\theta_t)\|^2] = \bar{p}_{\text{eff}} \sum_{t=1}^T \mathbb{E}[\|\nabla F(\theta_t)\|^2].$$

Dividing both sides by  $\frac{\eta}{2} \bar{p}_{\text{eff}} T$  yields Equation 35.  $\square$

**Iteration Complexity Extraction.** Let  $B_{\text{ours}}(T)$  denote the right-hand side of Equation 35. By Definition 17, the iteration complexity  $T_{\varepsilon}^{\text{ours}}$  is the smallest  $T$  such that  $B_{\text{ours}}(T) \leq \varepsilon$ .

Equivalently, if

$$\varepsilon > \frac{L\eta}{\bar{p}_{\text{eff}}} \cdot \frac{\sigma^2}{M}, \quad (36)$$

which ensures that the target accuracy  $\varepsilon$  lies above the *noise floor* induced by stochastic gradient variance, then  $T_{\varepsilon}^{\text{ours}}$  admits the closed-form bound

$$T_{\varepsilon}^{\text{ours}} = \left\lceil \frac{2(F(\theta_1) - F^*)}{\bar{p}_{\text{eff}} \eta \left( \varepsilon - \frac{L\eta}{\bar{p}_{\text{eff}}} \cdot \frac{\sigma^2}{M} \right)} \right\rceil. \quad (37)$$

In the noise-free case  $\sigma = 0$ , the noise-floor term vanishes and Equation 37 simplifies to

$$T_{\varepsilon}^{\text{ours}} = \left\lceil \frac{C}{\bar{p}_{\text{eff}} \varepsilon} \right\rceil, \quad (38)$$

where  $C := \frac{2(F(\theta_1) - F^*)}{\eta}$  is independent of freezing.

#### D.1.5. COMPARISON WITH NO-FREEZING BASELINE

For the no-freezing baseline, define  $\bar{g}_t := \frac{1}{M} \sum_{m=1}^M g_{t,m}$  and

$$\theta_{t+1} = \theta_t - \eta \bar{g}_t. \quad (39)$$

Repeating the same argument (with  $\mathbb{U}_{t,m} \equiv \mathbf{1}$  and  $r_{\max} = 0$ ) yields, under  $\eta \leq \frac{1}{L(1+1/M)}$ ,

$$\frac{1}{T} \sum_{t=1}^T \mathbb{E}[\|\nabla F(\theta_t)\|^2] \leq \frac{2(F(\theta_1) - F^*)}{\eta T} + L\eta \cdot \frac{\sigma^2}{M}. \quad (40)$$

Accordingly, for  $\varepsilon$  satisfying

$$\varepsilon > L\eta \cdot \frac{\sigma^2}{M}, \quad (41)$$

$T_{\varepsilon}^{\text{base}}$  can be expressed as

$$T_{\varepsilon}^{\text{base}} = \left\lceil \frac{2(F(\theta_1) - F^*)}{\eta \left( \varepsilon - L\eta \cdot \frac{\sigma^2}{M} \right)} \right\rceil, \quad (42)$$

which can be simplified to

$$T_{\varepsilon}^{\text{ours}} = \left\lceil \frac{C}{\varepsilon} \right\rceil, \quad (43)$$

in the noise-free case  $\sigma = 0$ . (Note that  $C = \frac{2(F(\theta_1) - F^*)}{\eta}$ .)

**Corollary D.14** (Freeze-ratio Scaling). *In the noise-free case  $\sigma = 0$ , combining Equation 38 and Equation 43 yields*

$$T_\varepsilon^{\text{ours}} \approx \frac{1}{\bar{p}_{\text{eff}}} T_\varepsilon^{\text{base}}, \quad (44)$$

where  $\bar{p}_{\text{eff}} \in [1 - r_{\max}, 1]$  denotes the average effective update probability defined in Definition D.8.

That is, compared to the no-freezing baseline, TimelyFreeze increases the iteration complexity by a factor inversely proportional to the fraction of gradient energy that is effectively updated. In the worst case, this recovers the scaling  $T_\varepsilon^{\text{ours}} = \Theta(\frac{1}{1-r_{\max}} T_\varepsilon^{\text{base}})$ , while in typical regimes where  $\bar{p}_{\text{eff}} \gg 1 - r_{\max}$ , the resulting iteration complexity remains significantly tighter than the worst-case bound implied by  $r_{\max}$ .

More generally, when  $\sigma > 0$ , the above scaling continues to hold for the optimization term, up to the standard noise-floor effects in Equation 35 and Equation 40.

## D.2. Execution Time Analysis

We now analyze how parameter freezing affects the per-step execution time  $\tau_t^{\text{ours}}$  under TimelyFreeze, and relate the resulting speedup explicitly to the maximum freeze ratio  $r_{\max}$ .

**Remark on Progressive Freezing.** TimelyFreeze employs a *progressive freezing* strategy, under which the per-step execution time  $\tau_t^{\text{ours}}$  may vary during the transition phase. For analytical clarity, we focus on the *stable freezing regime*, where the freeze ratios have converged and the pipeline schedule becomes stationary, so that the per-step execution time can be well approximated by a constant  $\tau^{\text{ours}}$  (i.e.,  $\tau_t^{\text{ours}} \approx \tau^{\text{ours}}$  for all  $t$ ). This assumption is also practically justified, as the stable freezing regime dominates the overall training time in long-running jobs (see Figure 4).

**DAG-based Per-step Time Representation.** Recall that the per-step execution time is characterized by the makespan of the pipeline DAG (see Section 3.2.1). We therefore identify the per-step execution time with the critical-path length of the end-to-end graph,

$$\tau(\mathbf{r}) \equiv P_d(\mathbf{r}), \quad (45)$$

where  $P_d(\mathbf{r})$  denotes the longest-path value (i.e., the start time of the destination node) under a freezing decision  $\mathbf{r}$ .

**Upper and Lower Makespan Envelopes.** Given the measured execution-time bounds  $w_i^{\min}$  and  $w_i^{\max}$  for each action block  $i$ , we define the corresponding makespan envelopes as

$$P_d^{\min} := P_d(\mathbf{1}), \quad P_d^{\max} := P_d(\mathbf{0}), \quad (46)$$

where  $P_d(\cdot)$  denotes the longest-path operator on the DAG. Here,  $P_d(\mathbf{1})$  corresponds to the case where all parameters are frozen ( $r_i = 1$  and  $w_i = w_i^{\min}$  for all action nodes  $i$ ), while  $P_d(\mathbf{0})$  corresponds to the no-freezing case ( $r_i = 0$  and  $w_i = w_i^{\max}$  for all action nodes  $i$ ). Accordingly, the no-freezing baseline satisfies

$$\tau^{\text{base}} = P_d^{\max}. \quad (47)$$

Since freezing primarily reduces the backward-related portion of execution time, we approximate the achievable makespan reduction as scaling linearly with the maximum freeze ratio  $r_{\max}$ . Specifically, we interpolate between the two makespan envelopes as

$$\tau^{\text{ours}} \approx P_d^{\max} - r_{\max}(P_d^{\max} - P_d^{\min}) = P_d^{\min} + (1 - r_{\max})(P_d^{\max} - P_d^{\min}). \quad (48)$$

This approximation is most accurate when (i) the critical path is dominated by backward computation and (ii) the identity of the bottleneck path does not change significantly under freezing.

### D.2.1. COMPARISON WITH NO-FREEZING BASELINE

Combining the baseline Equation 47 and TimelyFreeze Equation 48, we obtain

$$\frac{\tau^{\text{ours}}}{\tau^{\text{base}}} \approx \frac{P_d^{\min} + (1 - r_{\max})(P_d^{\max} - P_d^{\min})}{P_d^{\max}}. \quad (49)$$

For simplicity, we define the time-reduction factor

$$\kappa := \frac{\tau^{\text{ours}}}{\tau^{\text{base}}} \approx (1 - r_{\max}) + r_{\max} \frac{P_d^{\min}}{P_d^{\max}}, \quad (50)$$

where  $\kappa \in (0, 1]$ . This expression makes explicit how the achievable per-step speedup depends on both the maximum freeze ratio  $r_{\max}$  and the gap between the upper and lower makespan envelopes. Intuitively, when backward computation dominates the critical path, the per-step execution time decreases nearly proportionally to  $1 - r_{\max}$ , whereas the irreducible forward and pipeline overheads limit the speedup as  $P_d^{\min}/P_d^{\max}$  increases.

### D.3. Time-to-Accuracy Comparison

We combine the iteration complexity analysis (Section D.1) and the per-step execution time analysis (Section D.2) to characterize the end-to-end *time-to-accuracy* (TTA).

In the stable freezing regime, the per-step execution time can be approximated by a constant  $\tau^{\text{alg}}$ , with  $\tau^{\text{base}} = P_d^{\max}$  for the no-freezing baseline. Accordingly, the TTA definition in Equation 14 admits the approximation

$$\text{TTA}_{\varepsilon}^{\text{alg}} \approx T_{\varepsilon}^{\text{alg}} \cdot \bar{\tau}^{\text{alg}}, \quad (51)$$

where  $T_{\varepsilon}^{\text{alg}}$  denotes a sufficient number of training steps given by the convergence bound.

**Theorem D.15** (Noise-free TTA Comparison). *In the noise-free case  $\sigma = 0$ , under the stable-regime approximation Equation 51, suppose the iteration complexity and per-step execution time satisfy*

$$T_{\varepsilon}^{\text{ours}} \approx \frac{1}{\bar{p}_{\text{eff}}} T_{\varepsilon}^{\text{base}} \quad (\text{cf. Corollary D.14}), \quad (52)$$

and

$$\kappa := \frac{T_{\varepsilon}^{\text{ours}}}{\tau^{\text{base}}} \approx (1 - r_{\max}) + r_{\max} \frac{P_d^{\min}}{P_d^{\max}} \quad (\text{cf. Equation 50}). \quad (53)$$

Then the time-to-accuracy ratio admits the approximation

$$\frac{\text{TTA}_{\varepsilon}^{\text{ours}}}{\text{TTA}_{\varepsilon}^{\text{base}}} \approx \frac{\kappa}{\bar{p}_{\text{eff}}}. \quad (54)$$

In particular, if

$$\kappa < \bar{p}_{\text{eff}}, \quad (55)$$

then TimelyFreeze strictly improves wall-clock time-to-accuracy, i.e.,

$$\text{TTA}_{\varepsilon}^{\text{ours}} < \text{TTA}_{\varepsilon}^{\text{base}}.$$

*Proof.* By the approximation  $\text{TTA}_{\varepsilon}^{\text{alg}} \approx T_{\varepsilon}^{\text{alg}} \bar{\tau}^{\text{alg}}$ ,

$$\frac{\text{TTA}_{\varepsilon}^{\text{ours}}}{\text{TTA}_{\varepsilon}^{\text{base}}} \approx \frac{T_{\varepsilon}^{\text{ours}}}{T_{\varepsilon}^{\text{base}}} \cdot \frac{\tau^{\text{ours}}}{\tau^{\text{base}}} \approx \frac{1}{\bar{p}_{\text{eff}}} \cdot \kappa.$$

The improvement condition Equation 55 immediately follows.  $\square$

## E. Experiment Results

### E.1. Experiment Setting Details

The implementation code is available at <https://anonymous.4open.science/r/TimelyFreeze/>.

Table 3. Experimental setup for language and vision finetuning tasks.

Model	Language Tasks			Vision Tasks	
	LLaMA-3.2-1B	LLaMA-3-8B	LLaMA-2-13B	ConvNeXt-V2-L	ViT-L/32
Dataset	Alpaca-GPT4	OpenHermes-2.5	OpenHermes-2.5	Food-101	ImageNet-1K
GPU	4 × A6000	4 × H200	4 × H200	4 × RTX 3090	8 × RTX 3090
Seed	42, 22, 11	42, 22, 11	42	42	42
Training Steps	800	2,000	2,000	20,000	17,500
Warmup Steps	100	200	200	2,500	1,500
Optimizer	AdamW	AdamW	AdamW	AdamW	SGD
Learning Rate	5.0e-6	3.0e-6	3.0e-6	1e-4	3e-3
LR Scheduler	Cosine Annealing			Cosine Annealing	
Global Batch Size	128	64	64	64	512
Local Batch Size	16	16	16	64	512
Seq. Length / Image Size	1024	1024	1024	224 × 224	224 × 224
Pipeline Parallel Degree	4	4	4	4	8
Num. Microbatches	8	8	8	8	8
Phase Boundaries $T_w, T_m, T_f$	60, 100, 200	160, 200, 250	150, 200, 250	2350, 2850, 5600	1400, 1600, 2400
Max Freeze Ratio $r_{\max}$	0.8	0.8	0.8	0.5	0.8
APF Threshold $T_{APF}$	0.01	0.0001	0.0001	0.005	0.005
AutoFreeze Percentage $P_{Auto}$	80%	80%	80%	80%	80%

### E.2. LLaMA 1B Result Table

Table 4. Comparison of freezing methods across different pipeline schedules (Llama-3.2-1B). The average accuracy of the pretrained (no fine-tuning) baseline is 34.93. The best and second-best values among the five freezing methods (APF, AutoFreeze, TimelyFreeze, and two hybrid variants) are highlighted in bold and underline, respectively.

GPipe				1F1B					
Freeze Method	Accuracy Preservation		Time Efficiency		Freeze Method	Accuracy Preservation		Time Efficiency	
	Avg. Acc. (Δ)↑	Frz. Ratio	Throughput (Δ)↑	MFU↑		Avg. Acc. (Δ)↑	Frz. Ratio	Throughput (Δ)↑	MFU↑
No Freezing	36.70 (+0.00)	0.00	6965 (0.00)	16.05	No Freezing	35.91 (+0.00)	0.00	7152 (0.00)	16.48
APF	<b>35.86</b> (-0.84)	35.08	8183 (17.49)	18.81	APF	<b>35.73</b> (-0.18)	35.06	8223 (14.98)	18.91
AutoFreeze	35.78 (-0.92)	24.91	7536 (8.20)	17.34	AutoFreeze	34.51 (-1.41)	26.47	7624 (6.60)	17.54
TimelyFreeze	<b>36.64</b> (-0.06)	19.97	<u>8821</u> (26.64)	<u>20.27</u>	TimelyFreeze	<b>36.36</b> (+0.45)	15.53	<b>9257</b> (29.44)	<b>21.31</b>
+APF	36.18 (-0.53)	20.19	<b>8860</b> (27.21)	<b>20.41</b>	+APF	35.69 (-0.23)	15.36	9161 (28.09)	21.10
+AutoFreeze	<u>36.39</u> (-0.32)	19.49	8809 (26.47)	20.28	+AutoFreeze	35.09 (-0.83)	15.53	<u>9184</u> (28.42)	<u>21.16</u>
Interleaved 1F1B									
Freeze Method	Accuracy Preservation		Time Efficiency		Freeze Method	Accuracy Preservation		Time Efficiency	
	Avg. Acc. (Δ)↑	Frz. Ratio	Throughput (Δ)↑	MFU↑		Avg. Acc. (Δ)↑	Frz. Ratio	Throughput (Δ)↑	MFU↑
No Freezing	36.42 (+0.00)	0.00	6800 (0.00)	15.68	No Freezing	36.57 (+0.00)	0.00	7541 (0.00)	17.31
APF	<u>35.73</u> (-0.69)	69.45	7564 (11.24)	17.40	APF	<u>35.59</u> (-0.98)	65.64	9372 (24.29)	21.50
AutoFreeze	34.25 (-2.16)	45.96	7112 (4.60)	16.38	AutoFreeze	35.32 (-1.25)	26.93	7906 (4.85)	18.13
TimelyFreeze	35.52 (-0.90)	37.89	<u>8355</u> (22.87)	<u>19.23</u>	TimelyFreeze	<b>35.95</b> (-0.62)	39.65	<b>9426</b> (25.01)	<b>21.63</b>
+APF	35.36 (-1.06)	38.50	8277 (21.73)	19.06	+APF	35.16 (-1.42)	38.41	9284 (23.12)	21.32
+AutoFreeze	<b>36.13</b> (-0.28)	38.50	<b>8366</b> (23.04)	<b>19.25</b>	+AutoFreeze	<u>35.59</u> (-0.98)	39.28	<u>9402</u> (24.68)	<u>21.58</u>
ZBV									
Freeze Method	Accuracy Preservation		Time Efficiency		Freeze Method	Accuracy Preservation		Time Efficiency	
	Avg. Acc. (Δ)↑	Frz. Ratio	Throughput (Δ)↑	MFU↑		Avg. Acc. (Δ)↑	Frz. Ratio	Throughput (Δ)↑	MFU↑
No Freezing	36.57 (+0.00)	0.00	7541 (0.00)	17.31	No Freezing	36.57 (+0.00)	0.00	7541 (0.00)	17.31
APF	<u>35.59</u> (-0.98)	65.64	9372 (24.29)	21.50	APF	<u>35.59</u> (-0.98)	65.64	9372 (24.29)	21.50
AutoFreeze	35.32 (-1.25)	26.93	7906 (4.85)	18.13	AutoFreeze	35.32 (-1.25)	26.93	7906 (4.85)	18.13
TimelyFreeze	<b>35.95</b> (-0.62)	39.65	<b>9426</b> (25.01)	<b>21.63</b>	TimelyFreeze	<b>35.95</b> (-0.62)	39.65	<b>9426</b> (25.01)	<b>21.63</b>
+APF	35.16 (-1.42)	38.41	9284 (23.12)	21.32	+APF	35.16 (-1.42)	38.41	9284 (23.12)	21.32
+AutoFreeze	<u>35.59</u> (-0.98)	39.28	<u>9402</u> (24.68)	<u>21.58</u>	+AutoFreeze	<u>35.59</u> (-0.98)	39.28	<u>9402</u> (24.68)	<u>21.58</u>

Table 5. Comparison of freezing methods across different pipeline schedules (LLaMA-2-13B). The average accuracy of the pretrained (no fine-tuning) baseline is 46.73. The best and second-best values among the five freezing methods (APF, AutoFreeze, TimelyFreeze, and two hybrid variants) are highlighted in bold and underline, respectively.

GPipe					1F1B					
Freeze Method	Accuracy Preservation		Time Efficiency			Freeze Method	Accuracy Preservation		Time Efficiency	
	Avg. Acc. ( $\Delta$ ) $\uparrow$	Frz. Ratio	Throughput ( $\Delta$ ) $\uparrow$	MFU $\uparrow$	Avg. Acc. ( $\Delta$ ) $\uparrow$		Frz. Ratio	Throughput ( $\Delta$ ) $\uparrow$	MFU $\uparrow$	
No Freezing	51.09 (0.00)	0.00	3550 (0.00)	27.40	No Freezing	51.15 (0.00)	0.00	3917 (0.00)	30.23	
APF	<b>50.14 (-0.94)</b>	60.75	<b>4819 (35.73)</b>	37.65	APF	<b>50.31 (-0.83)</b>	60.80	<b>5378 (37.31)</b>	42.08	
AutoFreeze	<b>50.23 (-0.86)</b>	84.45	<b>4989 (40.52)</b>	39.11	AutoFreeze	<b>50.21 (-0.94)</b>	87.64	<b>5660 (44.51)</b>	<b>44.26</b>	
TimelyFreeze	<b>50.81 (-0.28)</b>	72.18	<b>5132 (44.54)</b>	40.13	TimelyFreeze	<b>51.06 (-0.09)</b>	69.33	<b>5590 (42.72)</b>	43.68	
+APF	<b>51.00 (-0.09)</b>	72.24	<b>5199 (46.44)</b>	<b>40.70</b>	+APF	<b>50.59 (-0.55)</b>	69.68	<b>5743 (46.63)</b>	<b>44.97</b>	
+AutoFreeze	<b>50.81 (-0.28)</b>	72.21	<b>5138 (44.73)</b>	40.19	+AutoFreeze	<b>50.52 (-0.63)</b>	69.65	<b>5584 (42.57)</b>	43.62	
Interleaved 1F1B										
Freeze Method	Accuracy Preservation		Time Efficiency			Freeze Method	Accuracy Preservation		Time Efficiency	
	Avg. Acc. ( $\Delta$ ) $\uparrow$	Frz. Ratio	Throughput ( $\Delta$ ) $\uparrow$	MFU $\uparrow$	Avg. Acc. ( $\Delta$ ) $\uparrow$		Frz. Ratio	Throughput ( $\Delta$ ) $\uparrow$	MFU $\uparrow$	
No Freezing	50.90 (0.00)	0.00	4271 (0.00)	32.97	No Freezing	50.22 (0.00)	0.00	4660 (0.00)	35.97	
APF	<b>49.62 (-1.28)</b>	62.47	<b>5851 (36.99)</b>	<b>45.72</b>	APF	<b>49.77 (-0.45)</b>	45.23	<b>5945 (27.58)</b>	<b>46.16</b>	
AutoFreeze	<b>48.58 (-2.32)</b>	84.46	<b>5992 (40.29)</b>	<b>46.96</b>	AutoFreeze	<b>49.91 (-0.31)</b>	27.76	<b>4888 (4.90)</b>	37.76	
TimelyFreeze	<b>49.71 (-1.19)</b>	72.22	<b>5775 (35.22)</b>	44.95	TimelyFreeze	<b>50.36 (+0.14)</b>	63.42	<b>5809 (24.67)</b>	<b>45.03</b>	
+APF	<b>50.37 (-0.53)</b>	72.35	<b>5616 (31.50)</b>	43.65	+APF	<b>48.69 (-1.53)</b>	63.48	<b>5796 (24.37)</b>	44.92	
+AutoFreeze	<b>49.87 (-1.04)</b>	71.71	<b>5600 (31.12)</b>	43.52	+AutoFreeze	<b>49.62 (-0.61)</b>	63.51	<b>5791 (24.28)</b>	44.89	

### E.3. LLaMA Series Benchmark Results

Table 6. Detailed Benchmark Scores under different pipeline schedules (Llama-3.2-1B).

Base Pretrained Model					
Freeze Method	MMLU (5 shots)	HellaSwag (0 shots)	ARC-C (10 shots)	TruthQA (0 shots)	Avg. Acc. $\uparrow$
	31.99	47.75	36.95	23.01	34.93
GPipe					
Freeze Method	MMLU	HellaSwag	ARC-C	TruthQA	Avg.
No Freezing	32.04	49.15	37.63	27.99	36.70
APF	32.74	48.55	37.09	25.05	35.86
AutoFreeze	30.48	48.61	36.66	27.38	35.78
TimelyFreeze	<b>31.79</b>	<b>49.32</b>	<b>37.46</b>	<b>27.99</b>	<b>36.64</b>
+APF	31.32	49.04	37.37	26.97	36.18
+AutoFreeze	<b>31.56</b>	49.25	37.23	27.50	<b>36.39</b>
Interleaved 1F1B					
Freeze Method	MMLU	HellaSwag	ARC-C	TruthQA	Avg.
No Freezing	30.90	49.66	37.97	27.13	36.42
APF	32.55	48.35	36.89	25.13	<b>35.73</b>
AutoFreeze	28.39	44.53	37.65	26.44	34.25
TimelyFreeze	28.79	49.08	38.08	26.11	35.52
+APF	28.61	49.06	37.85	25.91	35.36
+AutoFreeze	30.42	49.36	38.31	26.44	<b>36.13</b>
1F1B					
Freeze Method	MMLU	HellaSwag	ARC-C	TruthQA	Avg.
No Freezing	30.42	49.34	37.57	26.32	35.91
APF	32.52	48.39	36.77	25.25	<b>35.73</b>
AutoFreeze	29.15	44.61	37.63	26.65	34.51
TimelyFreeze	31.30	<b>49.49</b>	37.80	26.85	<b>36.36</b>
+APF	29.66	49.26	37.51	26.32	35.69
+AutoFreeze	28.15	48.94	37.17	26.07	35.09
ZBV					
Freeze Method	MMLU	HellaSwag	ARC-C	TruthQA	Avg.
No Freezing	31.57	49.72	38.03	26.97	36.57
APF	32.33	48.24	37.23	24.56	<b>35.59</b>
AutoFreeze	29.10	48.08	37.63	26.48	35.32
TimelyFreeze	29.47	49.29	38.20	26.84	<b>35.95</b>
+APF	27.99	48.94	38.11	25.58	35.16
+AutoFreeze	29.09	49.14	38.00	26.15	<b>35.59</b>

Table 7. Detailed Benchmark Scores under different pipeline schedules (Llama-3-8B).

Base Pretrained Model					
Freeze Method	MMLU (5 shots)	HellaSwag (0 shots)	ARC-C (10 shots)	TruthfulQA (0 shots)	Avg. Acc. $\uparrow$
	63.55	60.00	51.28	28.40	50.81
GPipe					
Freeze Method	MMLU	HellaSwag	ARC-C	TruthQA	Avg.
No Freezing	64.09	61.45	55.63	37.33	54.63
APF	64.09	61.44	55.12	37.94	54.65
AutoFreeze	64.39	61.74	54.44	35.37	53.99
TimelyFreeze	63.44	61.73	55.86	38.15	54.79
+APF	63.27	61.60	56.45	37.94	<b>54.82</b>
+AutoFreeze	63.60	61.75	55.35	37.90	54.65
Interleaved 1F1B					
Freeze Method	MMLU	HellaSwag	ARC-C	TruthQA	Avg.
No Freezing	63.83	61.08	55.89	38.31	54.78
APF	64.72	61.53	55.89	37.82	<b>54.99</b>
AutoFreeze	64.34	61.29	55.20	37.33	54.54
TimelyFreeze	64.37	61.41	55.35	37.41	54.64
+APF	64.29	61.56	55.63	37.37	54.71
+AutoFreeze	64.40	61.54	55.29	37.66	54.72
1F1B					
Freeze Method	MMLU	HellaSwag	ARC-C	TruthQA	Avg.
No Freezing	64.09	61.45	55.63	37.33	54.63
APF	64.09	61.44	55.12	37.94	54.65
AutoFreeze	64.39	61.74	54.44	35.37	53.99
TimelyFreeze	64.02	61.39	55.94	37.41	54.69
+APF	64.36	61.51	55.58	37.90	<b>54.84</b>
+AutoFreeze	64.00	61.48	55.60	38.19	54.82
ZBV					
Freeze Method	MMLU	HellaSwag	ARC-C	TruthQA	Avg.
No Freezing	63.91	61.36	55.55	37.82	54.66
APF	64.56	61.65	55.55	36.11	54.47
AutoFreeze	63.64	61.48	56.23	38.07	54.86
TimelyFreeze	63.89	61.59	55.26	38.15	54.72
+APF	64.15	61.76	55.72	38.47	<b>55.03</b>
+AutoFreeze	63.97	61.64	56.40	38.19	<b>55.05</b>

Table 8. Detailed Benchmark Scores under different pipeline schedules (Llama-2-13B).

Base Pretrained Model					
Freeze Method	MMLU (5 shots)	HellaSwag (0 shots)	ARC-C (10 shots)	TruthfulQA (0 shots)	Avg. Acc. $\uparrow$
	52.38	60.18	47.53	26.81	46.73
GPipe					
Freeze Method	MMLU	HellaSwag	ARC-C	TruthQA	Avg.
No Freezing	56.33	60.33	54.27	33.41	51.09
APF	55.03	60.35	53.24	31.95	50.14
AutoFreeze	54.89	60.41	53.41	32.19	50.23
TimelyFreeze	55.21	60.76	54.69	32.56	<b>50.81</b>
+APF	54.81	60.95	54.69	33.54	<b>51.00</b>
+AutoFreeze	55.76	61.33	53.58	32.56	50.81
Interleaved 1F1B					
Freeze Method	MMLU	HellaSwag	ARC-C	TruthQA	Avg.
No Freezing	55.68	59.98	53.67	34.27	50.90
APF	55.36	60.44	50.85	31.82	49.62
AutoFreeze	54.76	57.89	54.61	27.05	48.58
TimelyFreeze	54.91	60.43	51.79	31.70	49.71
+APF	55.24	60.62	52.82	32.80	<b>50.37</b>
+AutoFreeze	54.45	60.48	53.07	31.46	<b>49.87</b>
1F1B					
Freeze Method	MMLU	HellaSwag	ARC-C	TruthQA	Avg.
No Freezing	55.57	60.71	54.27	34.03	51.15
APF	55.24	60.34	52.99	32.68	50.31
AutoFreeze	53.07	59.29	53.58	34.88	50.21
TimelyFreeze	55.71	60.22	55.12	33.17	<b>51.06</b>
+APF	55.78	60.82	52.47	33.29	<b>50.59</b>
+AutoFreeze	55.68	60.72	52.73	32.93	50.52
ZBV					
Freeze Method	MMLU	HellaSwag	ARC-C	TruthQA	Avg.
No Freezing	55.59	60.17	52.56	32.56	50.22
APF	55.22	59.98	52.05	31.82	49.77
AutoFreeze	55.60	60.60	53.07	30.35	<b>49.91</b>
TimelyFreeze	55.43	60.53	52.90	32.56	<b>50.36</b>
+APF	54.21	59.37	51.19	29.99	48.69
+AutoFreeze	55.59	60.23	50.94	31.70	49.62

## F. Pipeline Schedule Visualization

### F.1. Four-GPU Pipeline Schedules

Figure 7 presents example pipeline schedules for training the Llama-3-8B model using the GPipe schedule with eight microbatches on four H200 GPUs. This figure visualizes the pipeline schedules corresponding to the main results reported in Table 1. We compare three parameter-freezing methods—AutoFreeze, APF, and TimelyFreeze—against the baseline training without freezing. All freezing methods reduce the batch execution time to some extent; however, TimelyFreeze achieves the largest improvement, reducing the batch time by 31.66% relative to the baseline of 698 ms.

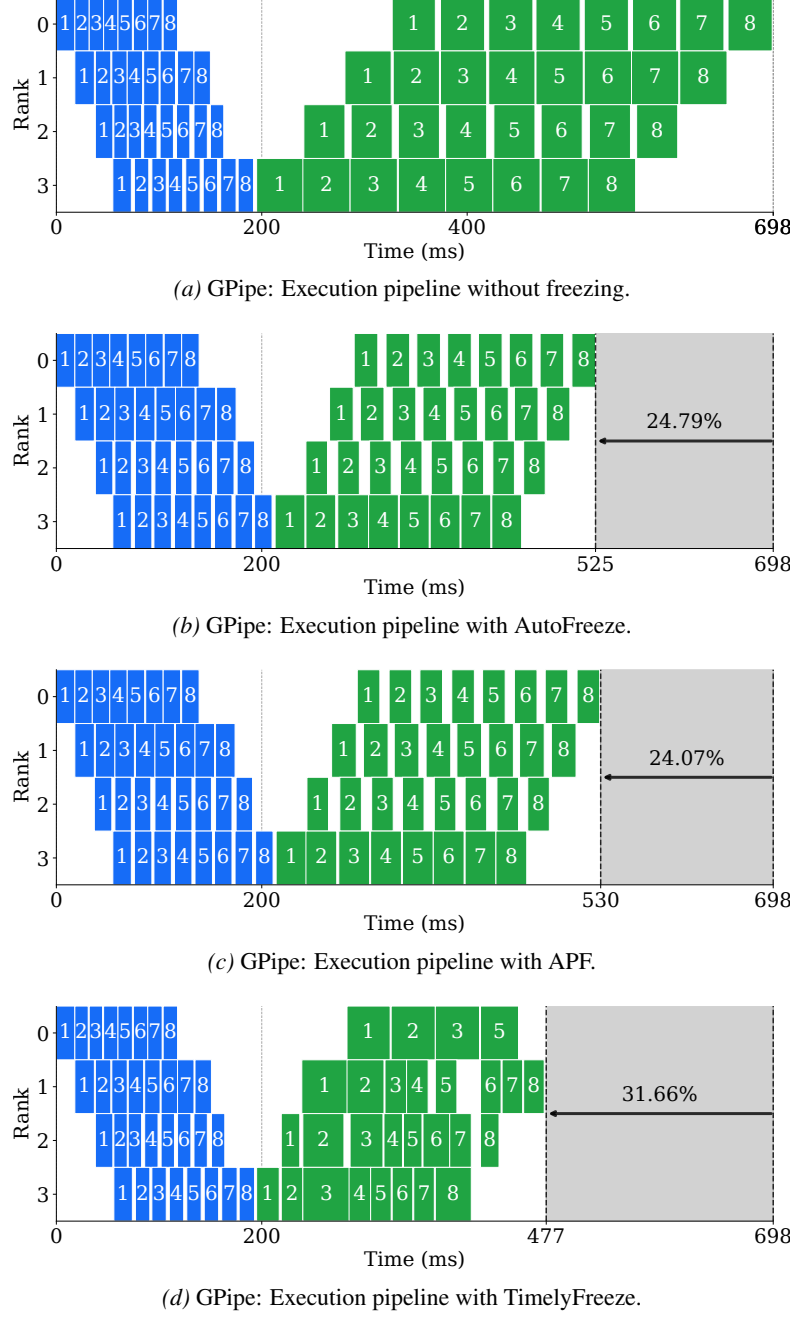
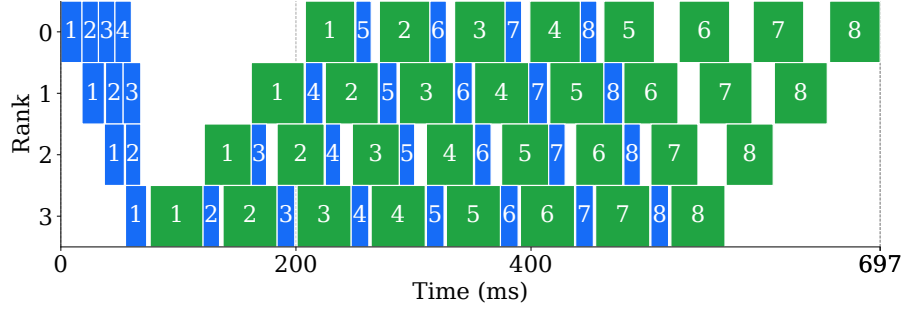
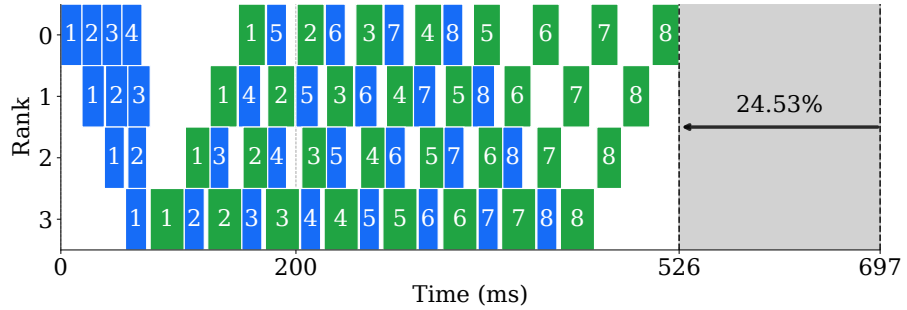


Figure 7. GPipe schedules across four freezing methods.

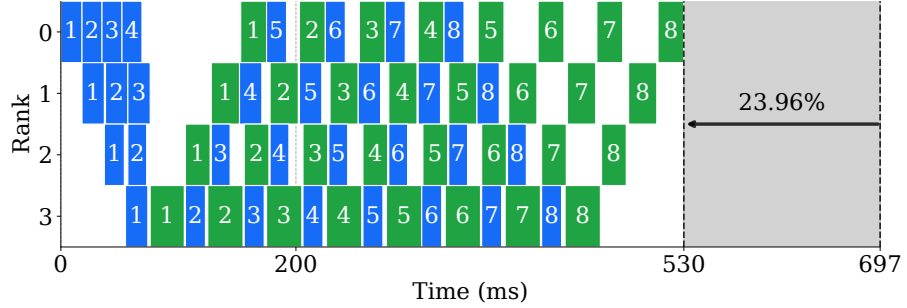
Figures 8 through 10 demonstrate consistent results across other pipeline schedules, including 1F1B, Interleaved 1F1B, and Zero-Bubble (ZBV).



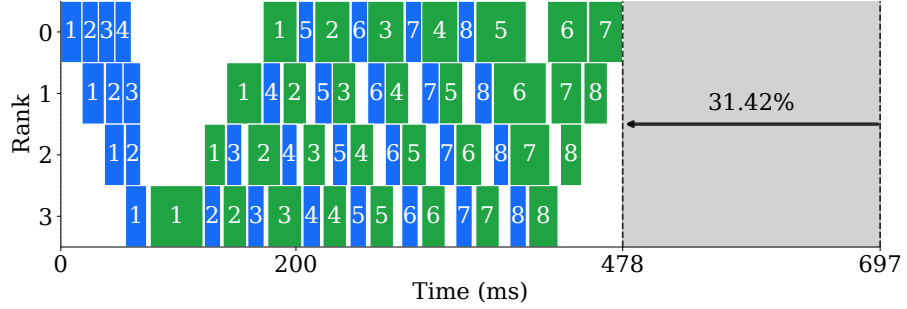
(a) 1F1B: Execution pipeline without freezing.



(b) 1F1B: Execution pipeline with AutoFreeze.

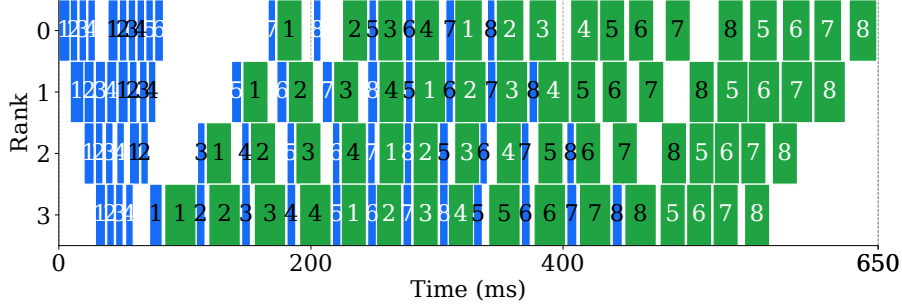


(c) 1F1B: Execution pipeline with APF.

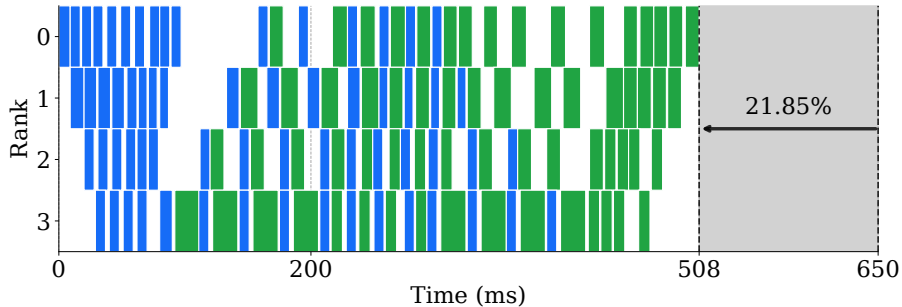


(d) 1F1B: Execution pipeline with TimelyFreeze.

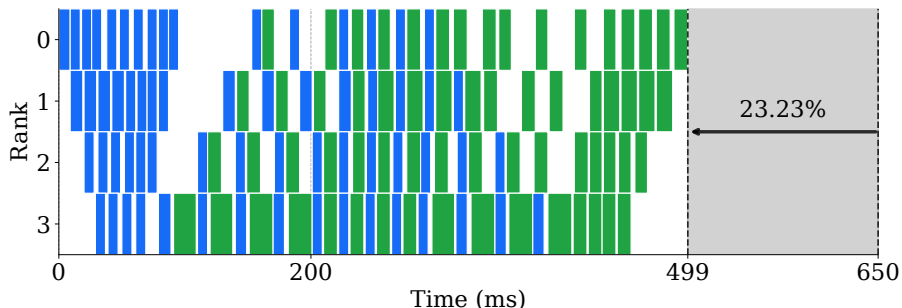
Figure 8. 1F1B schedules across four freezing methods.



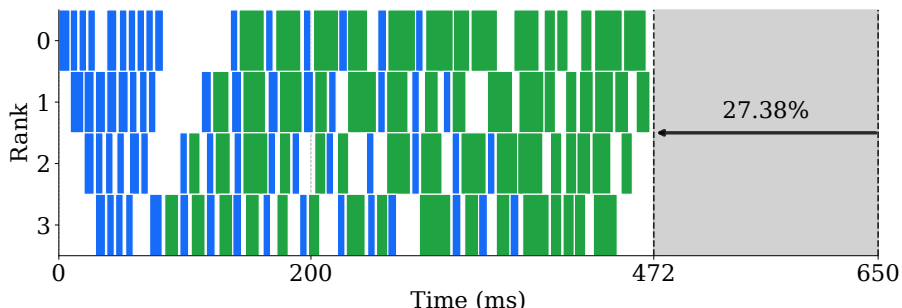
(a) Interleaved 1F1B: Execution pipeline without freezing.



(b) Interleaved 1F1B: Execution pipeline with AutoFreeze.

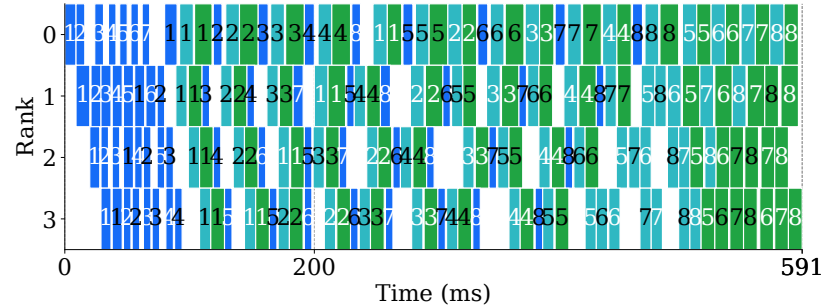


(c) Interleaved 1F1B: Execution pipeline with APF.

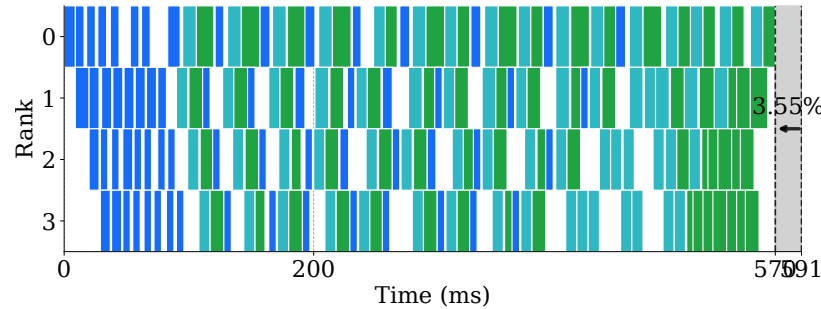


(d) Interleaved 1F1B: Execution pipeline with TimelyFreeze.

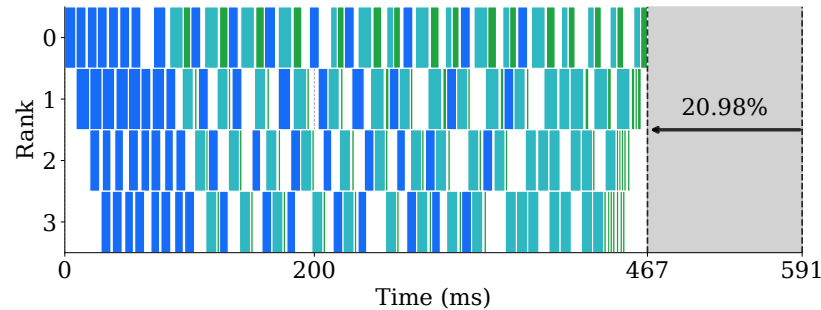
Figure 9. Interleaved 1F1B schedules across four freezing methods.



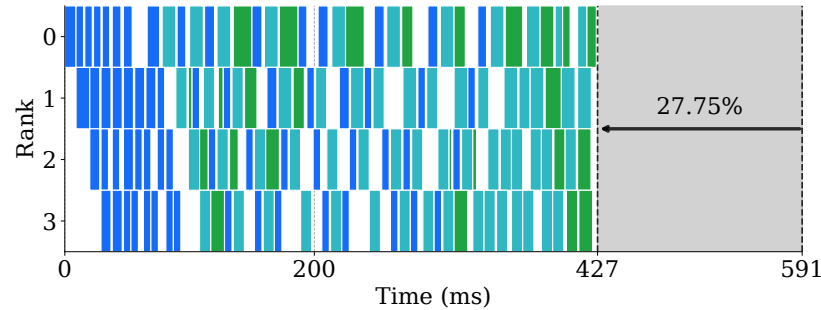
(a) ZBV: Execution pipeline without freezing.



(b) ZBV: Execution pipeline with AutoFreeze.



(c) ZBV: Execution pipeline with APF.



(d) ZBV: Execution pipeline with TimelyFreeze.

Figure 10. ZBV schedules across four freezing methods.

## F.2. 6-GPU Pipeline Schedules

Figures 11 and 12 present example pipeline schedules for training the Llama-3.2-1B model using the GPipe and 1F1B schedules with six microbatches on six A6000 GPUs. All other settings are identical to those used to obtain the results reported in Table 4.

Compared to the baseline without freezing, both APF and TimelyFreeze reduce the batch execution time; however, TimelyFreeze consistently achieves larger gains. In this setting, TimelyFreeze outperforms APF by up to 10 percentage points, which is notably higher than the 6–7 percentage point improvements observed in Figures 7 and 8. This result indicates that TimelyFreeze becomes increasingly effective as the degree of pipeline parallelism increases, where pipeline-level optimization plays a more critical role.

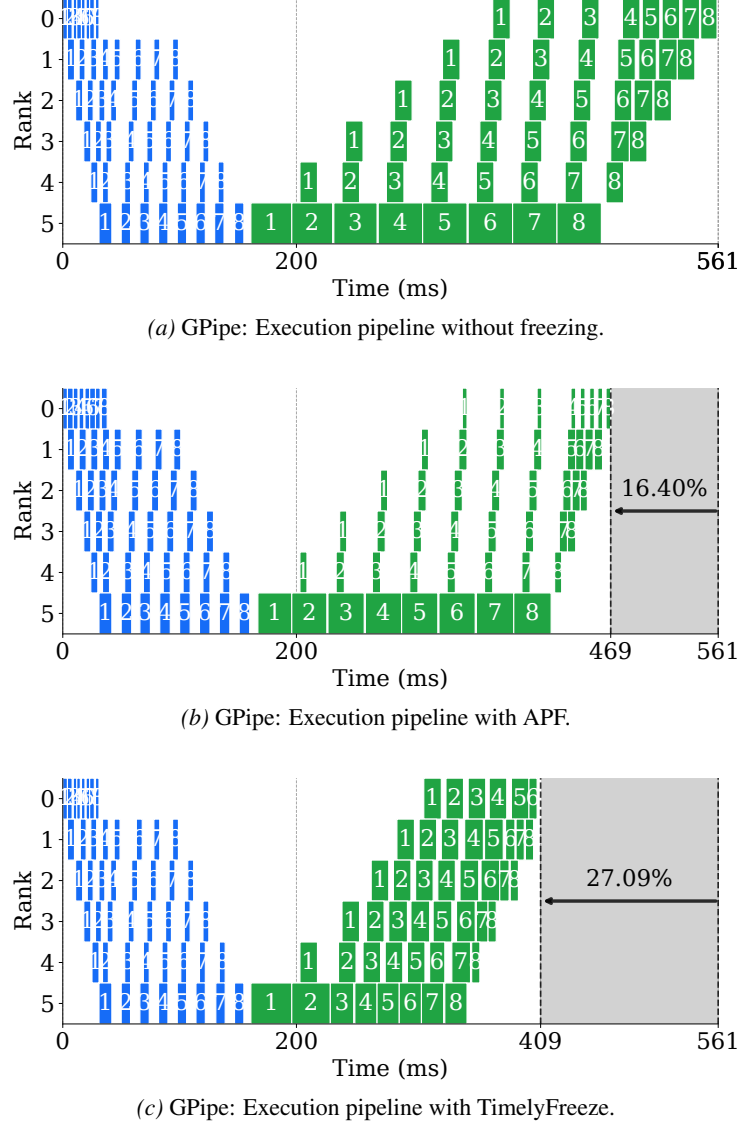
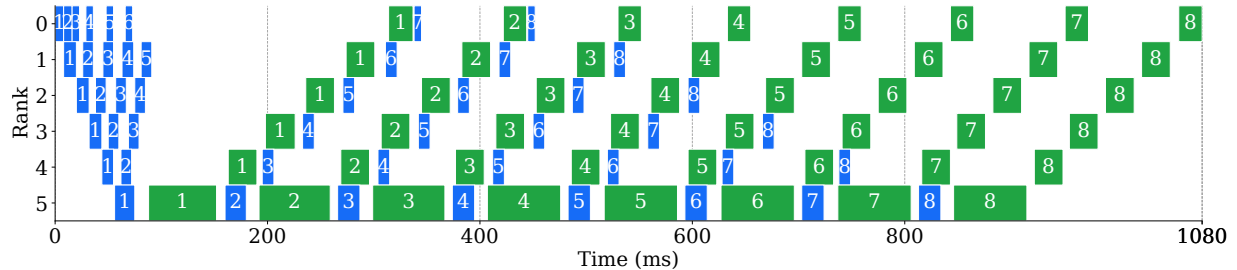
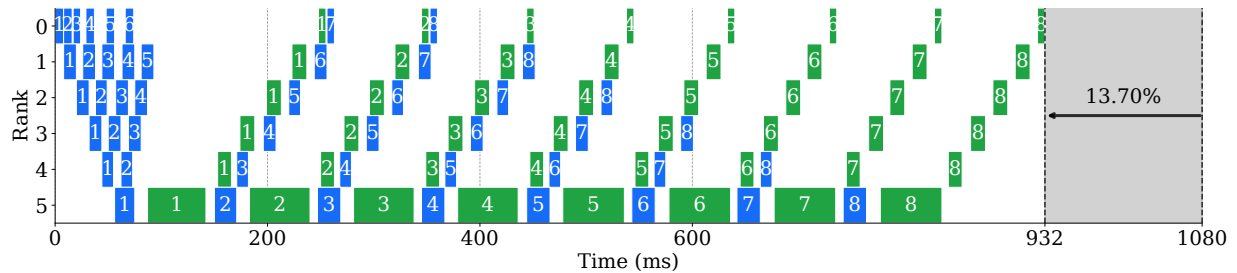


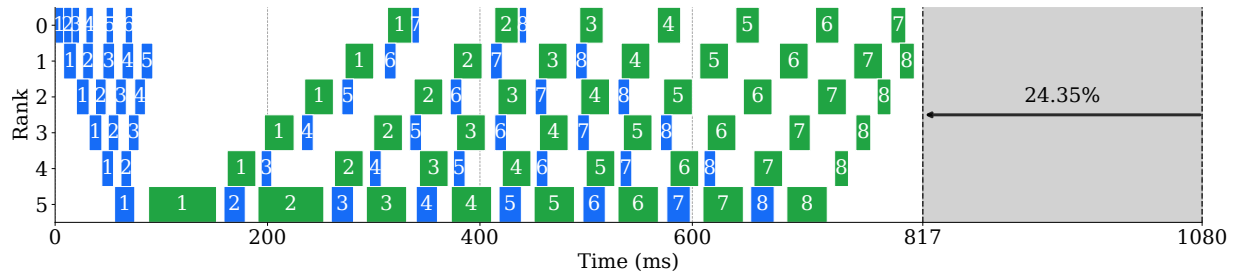
Figure 11. GPipe schedules across four freezing methods.



(a) 1F1B: Execution pipeline without freezing.

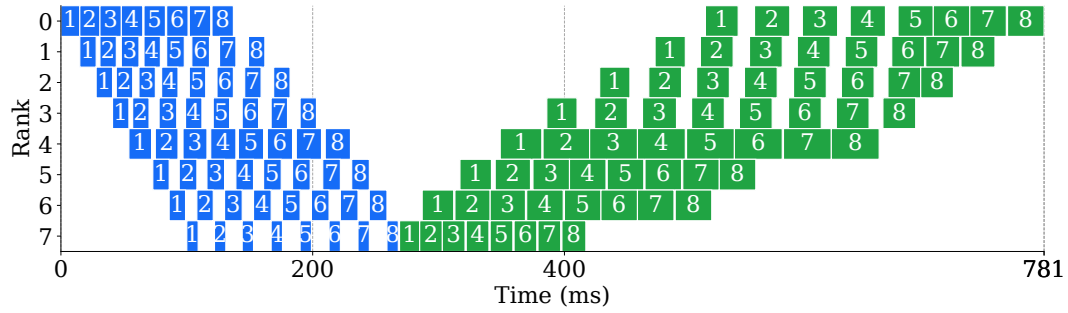


(b) 1F1B: Execution pipeline with APF.

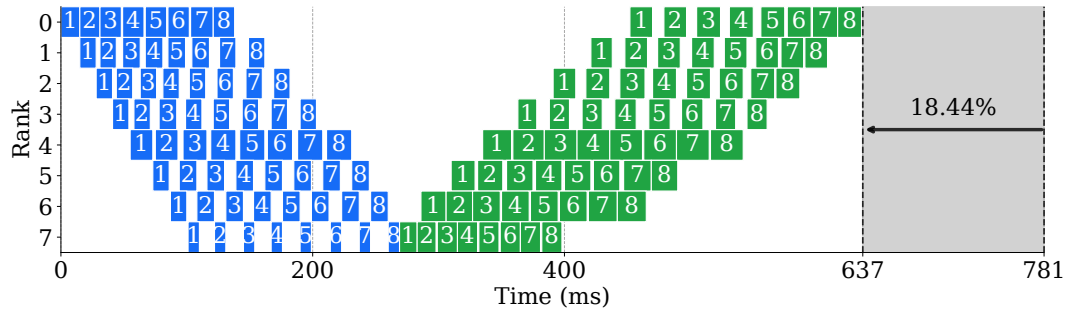


(c) 1F1B: Execution pipeline with TimelyFreeze.

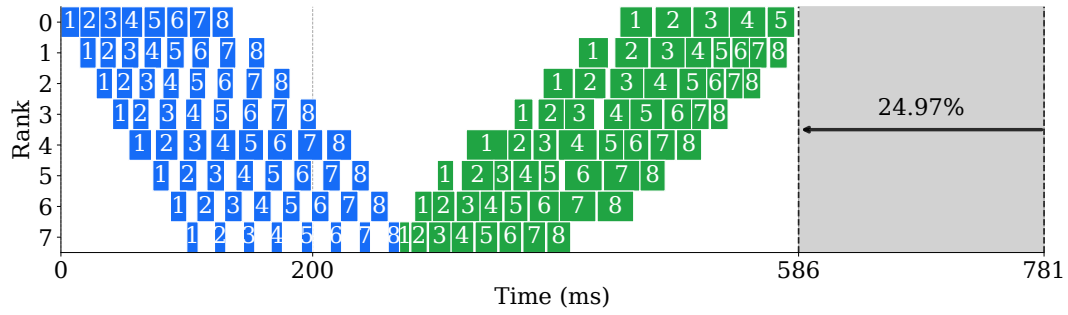
Figure 12. 1F1B schedules across freezing methods.

**F.3. 8-GPU Pipeline Schedules**


(a) GPipe: Execution pipeline without freezing.



(b) GPipe: Execution pipeline with APF.



(c) GPipe: Execution pipeline with TimelyFreeze.

Figure 13. GPipe schedules across freezing methods.

## G. Vision Model Results

TimelyFreeze also demonstrates strong generalization to image classification models, including ViT-L/32 and ConvNeXt-V2-L, which differ substantially from transformer LLMs in layer structure, operator heterogeneity, and training dynamics. Tables 9 and 10 summarize the results.

### G.1. ConvNeXt-V2-L Result Table

Table 9. Effect of freezing methods across partitioning heuristics and pipeline schedules. The best and second-best values among the three freezing methods (APF, AutoFreeze, and TimelyFreeze) are highlighted in bold and underline, respectively.

Partitioning Method	Freeze Method	GPipe			1F1B		
		Top1 Acc. ( $\Delta$ ) $\uparrow$	Train Time ( $\Delta$ ) $\downarrow$	Freeze Ratio	Top1 Acc. ( $\Delta$ ) $\uparrow$	Train Time ( $\Delta$ ) $\downarrow$	Freeze Ratio
Memory	No Freezing	87.00 (+0.00)	10507 (0.00)	0.00	91.57 (+0.00)	25212 (0.00)	0.00
	APF	84.50 <b>(-2.50)</b>	<b>8812</b> (16.13)	36.31	90.38 <b>(-1.19)</b>	<b>20784</b> (17.56)	36.92
	AutoFreeze	<b>86.17</b> (-0.83)	10256 (2.39)	21.57	<b>91.59</b> (+0.02)	24383 (3.29)	23.03
	TimelyFreeze	<u>85.53</u> (-1.47)	<u>8985</u> (14.49)	44.27	<u>90.76</u> (-0.81)	<u>21687</u> (13.98)	29.12
Parameter	No Freezing	86.28 (+0.00)	15144 (0.00)	0.00	91.59 (+0.00)	31935 (0.00)	0.00
	APF	85.13 <b>(-1.16)</b>	<b>12224</b> (19.28)	38.07	90.60 <b>(-0.99)</b>	<b>25397</b> (20.47)	36.66
	AutoFreeze	<b>87.03</b> (+0.75)	13202 (12.82)	10.38	<b>91.78</b> (+0.19)	27280 (14.58)	10.40
	TimelyFreeze	<u>86.47</u> (+0.19)	<u>11378</u> (24.87)	21.17	<u>91.04</u> (-0.55)	<b>24741</b> (22.53)	31.26
Time	No Freezing	86.92 (+0.00)	10476 (0.00)	0.00	91.67 (+0.00)	22820 (0.00)	0.00
	APF	84.80 <b>(-2.13)</b>	<u>8624</u> (17.68)	38.34	90.38 <b>(-1.30)</b>	<u>19220</u> (15.78)	37.10
	AutoFreeze	<b>86.61</b> (-0.31)	9751 (6.92)	23.11	<b>91.58</b> (-0.09)	21558 (5.53)	24.10
	TimelyFreeze	<u>85.80</u> (-1.13)	<b>8430</b> (19.53)	44.00	<u>91.28</u> (-0.40)	<b>18671</b> (18.18)	46.01

We evaluate TimelyFreeze under three widely used partitioning heuristics: *memory-based*, *parameter-based*, and *time-based*. Memory-based partitioning balances peak activation and parameter memory across devices and is commonly used when training near memory limits, where feasibility and OOM avoidance dominate. Parameter-based partitioning is the simplest and most widely adopted baseline: it requires no profiling and splits layers by parameter counts as a coarse proxy for compute and memory load. Time-based partitioning equalizes per-stage latency using backward (or forward–backward) timing profiles, and is typically preferred when wall-clock throughput is the primary concern.

### G.2. ViT-L/32 Result Table

Table 10. Finetuning results on ViT-L/32 with ImageNet-1K under different pipeline schedules.

Freeze Method	GPipe			1F1B		
	Top1 Acc. ( $\Delta$ ) $\uparrow$	Train Time ( $\Delta$ ) $\downarrow$	Freeze Ratio	Top1 Acc. ( $\Delta$ ) $\uparrow$	Train Time ( $\Delta$ ) $\downarrow$	Freeze Ratio
No Freezing	75.46 (+0.00)	14339 (0.00)	0.00	75.46 (+0.00)	13374 (0.00)	0.00
APF	42.07 <b>(-33.40)</b>	<u>12082</u> (15.74)	39.15	42.07 <b>(-33.40)</b>	<u>11305</u> (15.47)	39.71
AutoFreeze	<u>74.98</u> (-0.48)	13050 (8.99)	44.04	<u>74.98</u> (-0.48)	11991 (10.34)	44.04
TimelyFreeze	<b>75.03</b> (-0.44)	<b>11195</b> (21.93)	50.00	<b>75.04</b> (-0.42)	<b>10266</b> (23.24)	43.39

## H. Variation of Per-Parameter Freeze Ratios across Methods

Figure 14 compares the distributions of per-parameter freeze ratios across methods. TimelyFreeze exhibits a nearly uniform distribution, reflecting its schedule-driven and parameter-agnostic design. In contrast, APF produces highly skewed freeze ratios with large parameter-wise variance, while AutoFreeze shows pronounced layer-wise imbalances between early and late layers. The hybrid variants (TimelyFreeze+APF and TimelyFreeze+Auto) follow the trends of their metric-based counterparts but apply freezing more moderately, regularized by the stage-wise budgets computed by TimelyFreeze.

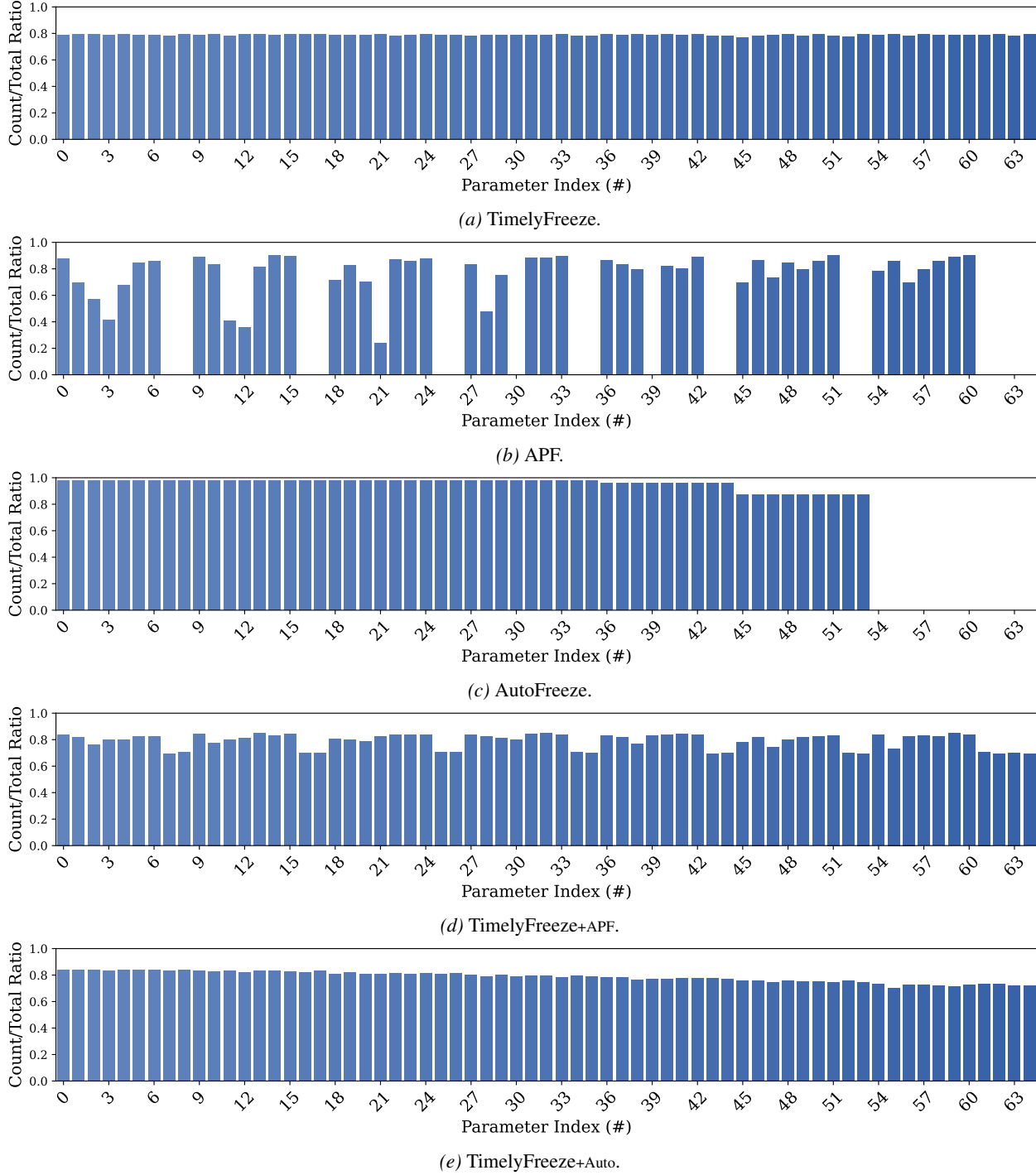
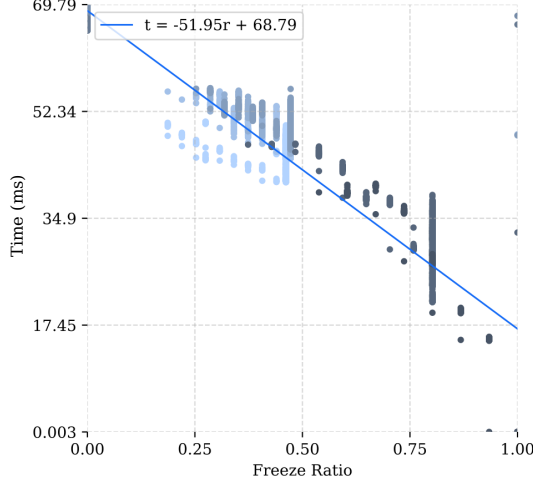
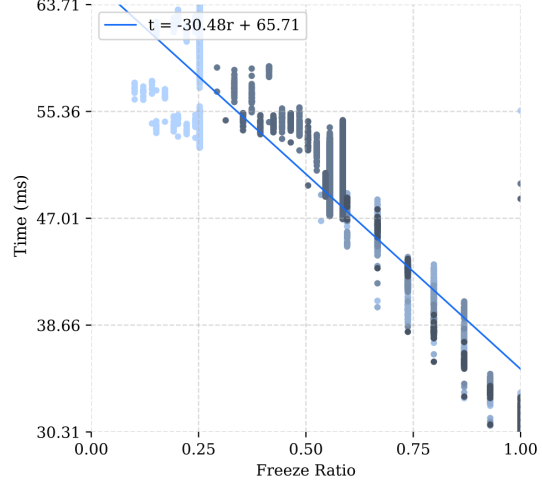


Figure 14. Frozen ratio histogram per parameter in Rank 3 with different methods.

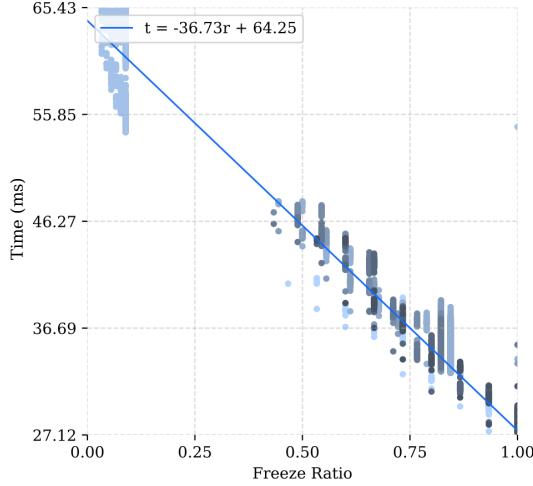
## I. Effect of Freeze Ratio on Backward Time



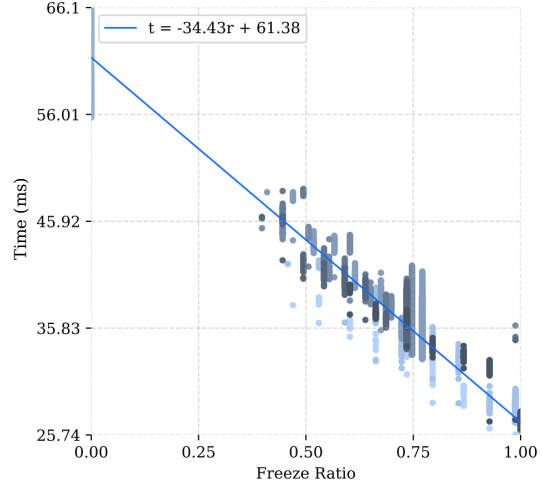
(a) Stage 0 (GPU Rank 0).



(b) Stage 1 (GPU Rank 1).



(c) Stage 2 (GPU Rank 2).



(d) Stage 3 (GPU Rank 3).

Figure 15. Backward computation time per effective freeze ratio across pipeline stages. Each subplot corresponds to a model stage (GPU rank 0–3). As the freeze ratio increases, the backward time decreases proportionally, verifying that TimelyFreeze dynamically modulates per-stage workload as designed. Blue markers indicate monitored microbatches, where color intensity reflects the microbatch index (lighter for earlier microbatches and darker for later ones).